Chapter 8

Structure of Finite Nuclei

The nuclear shell model, developed by Mayer and Jensen in 1952, is now a very successful and highly developed microscopic theory for the structure of finite nuclei. We will explore its basic aspects and illustrate its predictive power in this chapter.

We have previously seen that a successful description of nuclear matter can be obtained using a mean single particle potential and a weak residual N-N effective interaction. We will follow a similar strategy for finite nuclei. Assume that the Schrödinger equation can be written

$$\hat{H}\psi(1,2,\ldots A) = E\psi(1,2,\ldots A) \tag{8.1}$$

with the Hamiltonian given by

$$\hat{H} = \sum_i \Big(T_i + U(i) \Big) + \sum_{i<j} v_{ij} \,. \tag{8.2}$$

The single particle potential $U(i)$ and the residual two body interaction v_{ij} are both phenomenological, to be adjusted to reproduce the properties of real nuclei. Similar to the case of nuclear matter, we hope that if we find the "best" $U(i)$ then v_{ij} will be weak can be treated as a "perturbation".

8.1 Magic Nuclei, Single Particle States, And Spin-Orbit Interactions

As a first goal, we would hope to reproduce a basic systematic feature of the set of atomic nuclei: the "magic numbers". Empirically, it is found that there are large deviations from the smooth Bethe-Weizäcker formula for nuclear binding energies near certain "magic" values of N and Z. The nuclei with

$$Z, N = 2,\ 8,\ 20,\ 28,\ 50,\ 82,\ 126$$

have an excess of binding energy. This can be seen in Figure **??**.

Such a systematic feature should arise from the properties of the single particle potential $U(i)$, so we first work on the single particle potential. Let the Hamiltonian be

$$\hat{H} = \sum_i T_i + U(i) \,. \tag{8.3}$$

As a first attempt, let's explore the shell structure (or magic numbers) that result from a simple symmetric three dimensional harmonic oscillator potential.

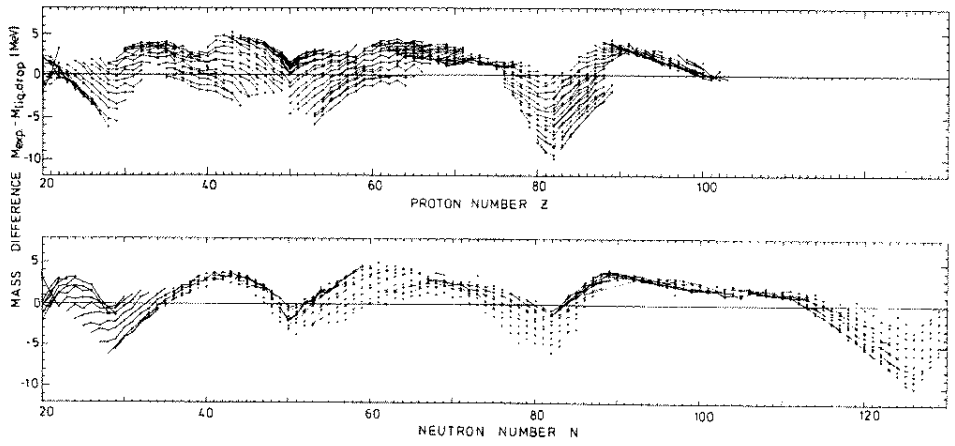

Figure 7.13. Nuclear (liquid drop) masses and the deviations with respect to the nuclear data and this, as a function of proton and neutron number. The shell closure effects are shown most dramatically (adapted from Myers 1966).

Figure 8.1: Binding energy of nuclides showing discontinuities at the magic numbers.

8.1.1 Harmonic Oscillator

The potential is given by

$$U(r_i) = \frac{1}{2}M\omega^2 r_i^2 \tag{8.4}$$

and ω can be adjusted to give the correct nuclear radius. We label the orbitals (eigenstates) by $\{\alpha, \beta, \ldots\}$. The energy of a particle in the orbital α is given by

$$E_\alpha = \left(n_\alpha + \frac{3}{2}\right)\hbar\omega \tag{8.5}$$

where n_α is an integer associated with the orbital α. Each n_α is the sum of three integers

$$n_\alpha = n_{\alpha x} + n_{\alpha y} + n_{\alpha z} \tag{8.6}$$

corresponding to the harmonic oscillator index associated with the three orthogonal axes of a Cartesion coordinate system. Each $n_{\alpha x}$ can take on the values 0,1,2, etc. So there are in general many different ways (each with a different orthogonal wave function) to make the index n_α by using different combinations for $n_{\alpha x}$, $n_{\alpha y}$, and $n_{\alpha z}$. The number of different combinations of integers is easily shown to be

$$\frac{(n_\alpha + 1)(n_\alpha + 2)}{2}\,. \tag{8.7}$$

First write out the integers 1, 2, ... n_α:

$$1 \quad 2 \quad 3 \quad 4 \quad \ldots \quad n_{\alpha-1} \quad n_\alpha$$

Then place 2 bars somewhere between the integers. There are $n_\alpha + 1$ places for the 1st bar, then $n_\alpha + 2$ places for the second. The number of integers to the left of the left-most bar is $n_{\alpha x}$, the number to the right of the right-most bar is $n_{\alpha z}$ and the number between is $n_{\alpha y}$. The number of ways to place the bars is

$$\frac{(n_\alpha + 1)(n_\alpha + 2)}{2} \tag{8.8}$$

where we divide by 2 since the bars can be interchanged to give the same result.

Now we fill the orbital α with the maximum number of particles, which is the degeneracy $(n_\alpha + 1)(n_\alpha + 2)/2$ times 4 (for spin and isospin). Then we fill all the orbitals n_α from 0 up to some maximum index $n_{\max}$ and count the number of particles:

$$A = 4 \times \sum_{n_\alpha=0}^{n_{\max}} \frac{(n_\alpha + 1)(n_\alpha + 2)}{2} = \frac{(n_{\max} + 1)(n_{\max} + 2)(n_{\max} + 3)}{6} \times 4 \tag{8.9}$$

We also can compute the nuclear radius to evaluate ω:

$$\frac{3}{5} r_0^2 A^{2/3} = \frac{4}{A} \cdot \sum_{n_\alpha=0}^{n_{\max}} \langle r_\alpha^2 \rangle \frac{(n_\alpha + 1)(n_\alpha + 2)}{2} \tag{8.10}$$

$$\langle r_\alpha^2 \rangle = \frac{\hbar}{M\omega}\left(n_\alpha + \frac{3}{2}\right); \quad \text{(virial theorem)} \tag{8.11}$$

$$\tag{8.12}$$

so we obtain

$$\hbar\omega = \frac{42}{A^{1/3}} \text{ MeV}. \tag{8.13}$$

There will be energy "gaps" between shell (orbital) fillings, when we finish filling each orbit. These occur at the values of

$$N, Z = \frac{(n+1)(n+2)(n+3)}{3}; \quad n = 0, 1, 2, \ldots \tag{8.14}$$

$$= 2, 8, 20, 40, 70, 112 \tag{8.15}$$

Although the first three numbers are a promising start, we find that this potential gives the wrong sequence of magic numbers.

8.1.2 Square Well

Next we try a square well for $U(\vec{r}_i)$. This more closely approximates the nuclear density, so should be a better choice for the mean potential.

$$U(r) = \begin{cases} -U_0 & 0 \le r \le R \\ 0 & r > R \end{cases}. \quad (U_0 > 0) \tag{8.16}$$

The interior region Schrödinger equation is

$$\vec{\nabla}^2 \phi_\alpha + 2M(U_0 - E_\alpha)\phi_\alpha = 0. \tag{8.17}$$

We define $k_\alpha^2 \equiv 2M(U_0 - E_\alpha)$ and write the solution in the form $\phi_\alpha = R_{nl}(r)Y_{lm}(\Omega)$ where the radial equation is

$$\frac{d^2R_{nl}}{dr^2} + \frac{2}{r}\frac{dR_{nl}}{dr} + \left[k_{nl}^2 - \frac{l(l+1)}{r^2}\right]R_{nl} = 0. \tag{8.18}$$

The solutions are the spherical Bessel ftns:

$$R_{nl} = j_l(k_{nl}r). \tag{8.19}$$

For a deep well, we require

$$j_l(k_{nl}R) = 0. \tag{8.20}$$

One can then find (see e.g., Abramowitz and Stegun, p. 467) the sequence of solutions shown in Table 8.1

k_{nl}R		2(2l+1)	Sum
π	l=0 (0s)	2	2
4.49	l=1 (0p)	6	8
5.79	l=2 (0d)	10	18
2π=6.28	l=0 (1s)	2	20
6.99	l=3 (0f)	14	34
7.22	l=1 (1p)	6	40

Table 8.1: Magic numbers for the square well potential.

Of course, a finite well will modify this sequence, but not drastically. So a square well cannot give the correct magic numbers either.

8.1.3 Spin-Orbit Potential

Many potentials have been tried, but none in fact none give the correct sequence of magic numbers. The only successful model uses a spin-orbit potential added to the central potential. A nucleon in the central region "sees" nucleons on all sides, moving in all directions, and with all spin orientations. Therefore, there would be no spin-orbit force contribution and we expect U(r)=constant, independent of $\vec{\sigma}$, $\vec{l}$. Thus, the spin orbit potential U_{so} is peaked at the nuclear surface, and is usually something like

$$U_{so}(r) = \frac{\gamma}{r}\frac{dU_{\rm cent}}{dr}(\vec{l}\cdot\vec{s}) = U_{LS}\vec{l}\cdot\vec{s} \tag{8.21}$$

since $\frac{dU_{\rm cent}}{dr}$ is only large at surface. The origin of this potential is associated with the exchange of vector mesons (such as the ρ meson) between nucleons.

It is easy to show that the splitting between orbitals with $j = l \pm \frac{1}{2}$ is given by a relation

$$\Delta E_{LS} = E_{j=l+\frac{1}{2}} - E_{j=l-\frac{1}{2}} = \langle U_{LS}\rangle\left(l + \frac{1}{2}\right). \tag{8.22}$$

$$\Delta E_{LS} = \langle U_{LS}\rangle\frac{1}{2}\left\{\left[j(j+1) - l(l+1) - \frac{3}{4}\right]_{l+\frac{1}{2}} - \left[j(j+1) - l(l+1) - \frac{3}{4}\right]_{l-\frac{1}{2}}\right\} \tag{8.23}$$

$$= \frac{1}{2}\langle U_{LS}\rangle\left[\left(l+\frac{1}{2}\right)\left(l+\frac{3}{2}\right)-\left(l-\frac{1}{2}\right)\left(l+\frac{1}{2}\right)\right] \tag{8.24}$$

$$= \langle U_{LS}\rangle\left(l+\frac{1}{2}\right) \tag{8.25}$$

We will see that $\langle U_{LS}\rangle < 0$ is the choice that gives the correct sign of the splitting.

Also, the Woods-Saxon potential is commonly used for the central potential:

$$U(r) = \frac{U_0}{1+e^{(r-c)/a_0}} \tag{8.26}$$

where a_0 = surface thickness parameter and c = radius parameter $\propto \mathrm{A}^{1/3}$. This central potential with the above spin-orbit potential gives the level sequence shown in Figure 8.2 which correctly reproduces the observed magic numbers.

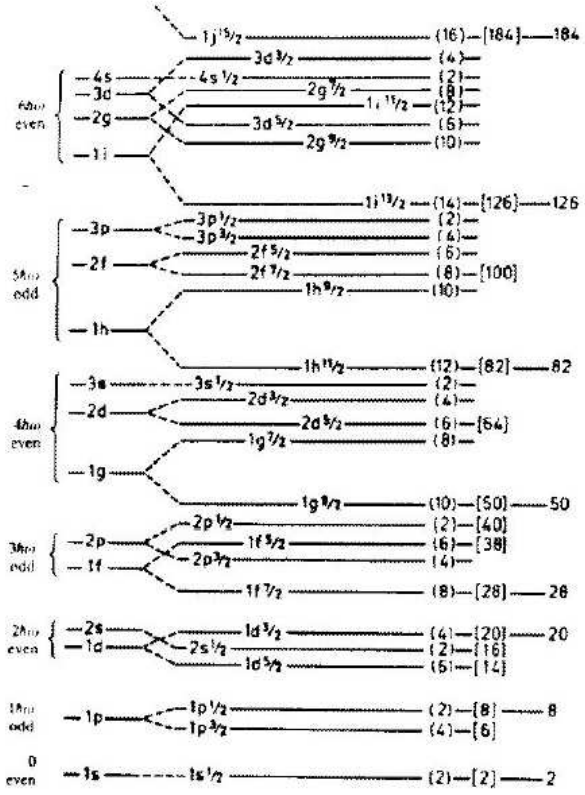

Figure 8.2: Energy level diagram for Woods-Saxon potential with spin-orbit force. The magic numbers are indicated on the right.

8.2 Nuclear Shell Model

The Woods-Saxon potential with a spin-orbit force is the mean-field that is the basis for the nuclear shell model. In addition, one can add residual interactions and correlations to produce more of the

details of the structure of nuclei. Here we confine ourselves to the basic features that one can study using the mean field potential.

8.2.1 Filled Orbitals

States associated with filled orbitals are the "magic" nuclei where Z or N is one of the magic numbers. Many nuclei with Z or N close to magic numbers can be treated with the filled orbital plus a few particles "holes". Consider an orbital with quantum numbers nlj which is filled with $2j+1$ particles, $m=-j, m=j+1, \ldots m=j-1, m=j$. Clearly we have

$$M = \sum_i m_i = 0.$$

The wave function can be written as a Slater determinant

$$\psi_{nlj} = \begin{vmatrix} \phi_{m=-j}(1) & \phi_{m=-j+1}(1) & \ldots \\ \phi_{-j}(2) & \phi_{-j+1}(2) & \ldots \end{vmatrix} \tag{8.27}$$

For each term we have

$$J_z \prod_i \phi_{m_i}(i) = 0. \tag{8.28}$$

In addition, the antisymmetry of ψ_{nlj} implies that, for each i, $J_\pm(i)\psi_{nlj} = 0$ so that $J_\pm \psi_{nlj} = 0$. Thus we have

$$J^2 = \frac{1}{2}(J_+ J_- + J_- J_+) + J_Z^2 = 0 \tag{8.29}$$

and so $J=0$ and $M=0$ for a filled orbital. The parity is given by $[(-)^l]^{2j+1}$. Since $2j+1$ must be an even integer, we obtain $\pi = +$. Therefore, a filled orbital has $J^\pi = 0^+$

8.2.2 Single particle in orbital

Now consider the case of a single particle in an orbital nlj.

$$J_z \phi_{nljm}(1) = m\phi_{nljm}(1) \tag{8.30}$$

$$J^2 \phi_{nljm} = j(j+1)\phi_{nljm} \tag{8.31}$$

So the total z component of angular momentum is

$$J_z^{\rm tot} = J_z|_{\rm filled} + J_z = J_z \tag{8.32}$$

and

$$\hat{J}^{\rm tot\,2} = \hat{J}^2|_{\rm filled} + 2\vec{J}_{\rm filled}\cdot\vec{J} + J^2 = J^2 \tag{8.33}$$

So we have $J=j$ and parity $\pi = (-)^l$.

8.2.3 Hole in orbital

We designate with Φ_{-1} the state with all levels filled except $nljm$. Then

$$J_z \Phi_{-1} = -m\Phi_{-1} \tag{8.34}$$

$$J^2 \Phi_{-1} = j(j+1)\Phi_{-1} \tag{8.35}$$

since we can couple Φ_{-1} and ϕ_{jm} to $J=0$.

8.2.4 2 Particles in Orbital

Now consider two particles in the states $nljm$ and $nljm'$. We can write a Slater determinant

$$\Phi(j^2, mm') = \frac{1}{\sqrt{2}} \begin{vmatrix} \phi_1(j,m) & \phi_1(j,m') \\ \phi_2(j,m) & \phi_2(j,m') \end{vmatrix} \tag{8.36}$$

and note the property $\Phi(j^2, mm') = -\Phi(j^2, m', m)$. We can use these to form a state of good angular momentum

$$\Phi(j^2, JM) = \sum_{m,m'} \langle jmjm'|JM\rangle \Phi(j^2, mm') \,. \tag{8.37}$$

Now use the symmetry of the Clebsch-Gordon coefficients:

$$\Phi(j^2, JM) = (-)^{2j-J} \sum \langle jm'jm|JM\rangle \Phi(j^2, mm') \tag{8.38}$$

$$= (-)^{2j-J+1} \sum \langle jmjm'|JM\rangle \Phi(j^2, m'm) \,. \tag{8.39}$$

The last line follows from the antisymmetry of the $\Phi(j^2, mm')$ and implies that $(-)^{2j-J+1} = +1$ or $(2j+1) - J =$ even. Since $2j+1$ is an even integer, we must have only even values of $J \leq 2j-1$.

Consider an example of two particles in an orbital, ^{18}O. This nucleus has $T = 1$ since it has two extra neutrons. The orbital for the neutrons is $d_{5/2}$ which implies the allowed levels will have $4^+, 2^+, 0^+$. Figure 8.4 shows that these are indeed the lowest three levels of ^{18}O. If we now consider ^{18}F (note $N = Z$), it also includes $1^+, 3^+, 5^+$ $T = 0$ states. These are those that are allowed for symmetric combinations of two nucleons in a $d_{5/2}$ orbital (the isospin state is antisymmetric for $T = 0$).

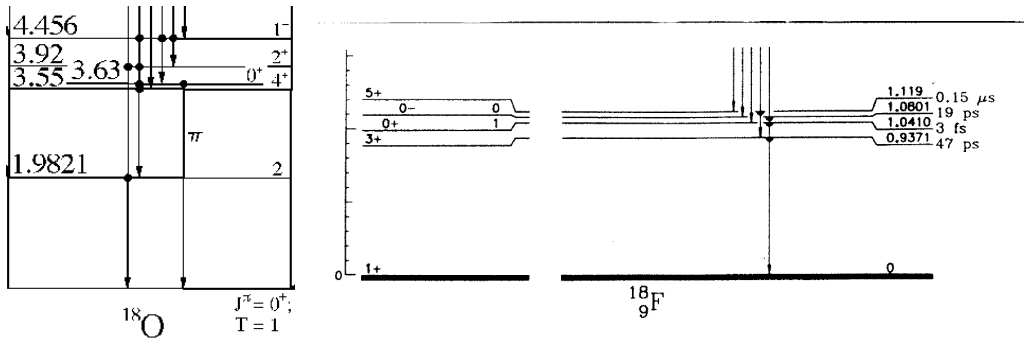

Figure 8.3: Energy level diagrams for ^{18}O (left) and ^{18}F (right).

8.2.5 Particle-hole combination

As an example of this situation, we consider ^{40}K which has $Z = 19$ and $N = 21$. Relative to ^{40}Ca (which is doubly magic), ^{40}K has a proton hole and a neutron particle. The proton hole is $d_{3/2}$ and the neutron is $f_{7/2}$, which we denote

$$(\pi d_{3/2})^{-1} (\nu f_{7/2}) \tag{8.40}$$

and the allowed spin-parity combinations are $5^-, 4^-, 3^-, 2^-$.

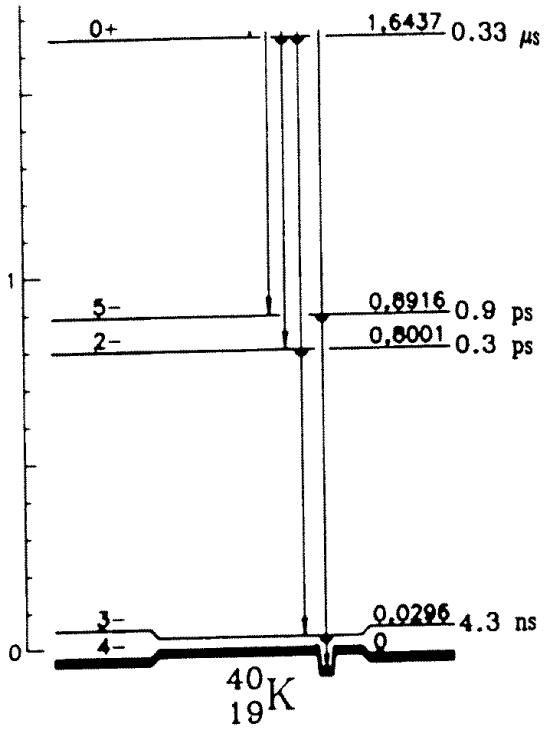

Figure 8.4: Energy level diagram for ^{40}K.

8.3 The 0p Shell

The simplest shell-model is the 0p shell. There is an inert ^{4}He core, and 2 single particle states to fill: $0P_{3/2}$ $0P_{1/2}$. The Hamiltonian is

$$\hat{H} = \hat{H}_0 + \frac{1}{2}\sum_{i\neq j} v_{ij} \tag{8.41}$$

and we will treat v_{ij} with perturbation theory. We first solve $\hat{H}_0\Psi_0 = E_0\Psi_0$ where

$$H_0 = \sum_i T_i + U_i \;\; ; \;\; U_i = U_C(x) + U_{LS}(x)(\vec{l}_i \cdot \vec{S}_i). \tag{8.42}$$

We can separate and solve the single particle problem

$$(T+U)\phi_\alpha = E_\alpha \phi_\alpha \tag{8.43}$$

where $\alpha = nljm$ with $l = 1$ and $n = 0$ only (0p shell). There are 2 possible j values, $j = l \pm \frac{1}{2}$, so we have $j = \frac{3}{2}$ and $\frac{1}{2}$. Since U is scalar, rotational invariance implies m degeneracy. Therefore, we have only 2 eigenvalues $E_{\frac{3}{2}}, E_{\frac{1}{2}}$ corresponding to $j = \frac{3}{2},\ \frac{1}{2}$.

α_1	α_2	T	J
$\frac{3}{2}$	$\frac{3}{2}$	T=1	2,0
$\frac{3}{2}$	$\frac{3}{2}$	T=0	3,1
$\frac{1}{2}$	$\frac{1}{2}$	T=1	0
$\frac{1}{2}$	$\frac{1}{2}$	T=0	1
$\frac{3}{2}$	$\frac{1}{2}$	T=1	2,1
$\frac{3}{2}$	$\frac{1}{2}$	T=0	2,1

Table 8.2: Two particle states allowed in the 0p shell.

For the solution of $\hat{H}$ with the v_{ij}, we need the 2-body matrix elements of the 0p shell. The allowed 2 nucleon states are shown in Table 8.2

There are 10 diagonal matrix elements, and there are the following off-diagonal elements:

$$\left\langle \frac{3}{2}\frac{3}{2}\ T=1, J=0 \left\| v \right\| \frac{1}{2}\frac{1}{2}\ T=1, J=0 \right\rangle \tag{8.44}$$

$$\left\langle \frac{3}{2}\frac{3}{2}\ T=0, J=1 \left\| v \right\| \frac{1}{2}\frac{1}{2}\ T=0, J=1 \right\rangle \tag{8.45}$$

$$\left\langle \frac{3}{2}\frac{3}{2}\ T=0, J=1 \left\| v \right\| \frac{3}{2}\frac{1}{2}\ T=0, J=1 \right\rangle \tag{8.46}$$

$$\left\langle \frac{1}{2}\frac{1}{2}\ T=0, J=1 \left\| v \right\| \frac{3}{2}\frac{1}{2}\ T=0, J=1 \right\rangle \tag{8.47}$$

$$\left\langle \frac{3}{2}\frac{3}{2}\ T=1, J=2 \left\| v \right\| \frac{3}{2}\frac{1}{2}\ T=1, J=2 \right\rangle \tag{8.48}$$

So there are 15 2-body matrix elements (15 real parameters) plus the 2 single particle energies - 17 parameters. Once these are determined, the p-shell problem is solved. The matrix elements are determined by diagonalizing each n-particle problem, $0 < n < 12$, and comparing energy differences with identified levels in real nuclei. Parameters are adjusted and the levels are recalculated until good convergence is achieved. Examples from a classic 1965 paper by Cohen and Kurath are shown in Figure 8.5.

8.4 Green's Function Monte Carlo and Other Methods

Green's function Monte Carlo is a numerical method solving the ground state of a few nucleon systems exactly, given two and three-body interaction potentials.

For heavy nuclei, the nuclear shell-model is too complicated because there are too many configurations that one has to take into account. In this case, the so-called density functional method can be used to solve the ground state.

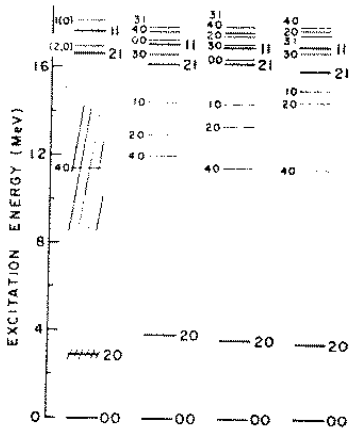

Fig. 3. The level scheme of Be^{8}. See caption of fig. 1 for details.

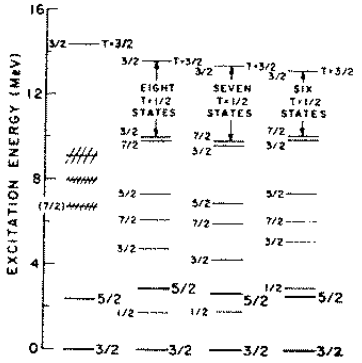

Fig. 4. The level scheme of Be^{9}. See caption of fig. 2 for details.

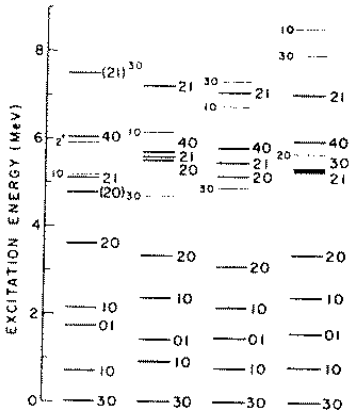

Fig. 5. The level scheme of B^{10}. See caption of fig. 1 for details.

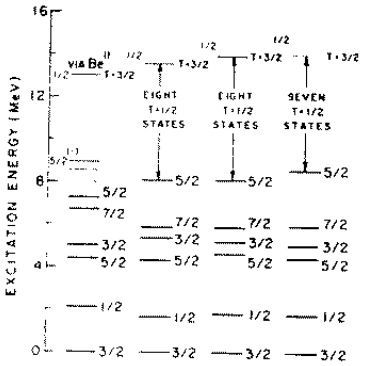

Fig. 6. The level scheme of B^{11}. See caption of fig. 2 for details.

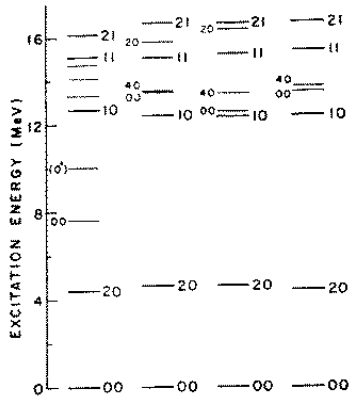

Fig. 7. The level scheme of C^{12}. See caption of fig. 1 for details.

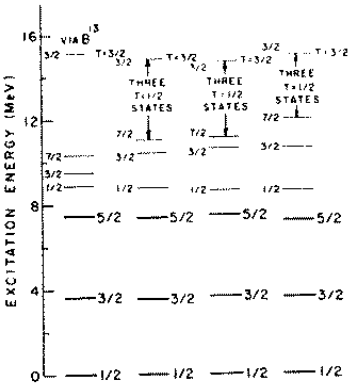

Fig. 8. The level scheme of N^{13}. See caption of fig. 2 for details.

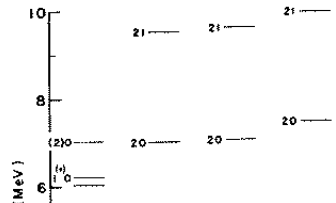

Chapter 9

Big-Bang Nucleosynthesis

After the universe cooled to a temperature of a few MeV, the energy density was still dominated by the large number of relativistic particles, all in thermal equilibrium: photons, electrons, positrons, neutrinos and antineutrinos. In addition there were the nucleons (neutrons and protons) that represent the baryonic matter that we observe today.

The number density of the gas of relativistic particles is given by (see Eq. 2.2):

$$n = g_n \frac{\zeta(3)}{\pi^2} T^3 \,. \tag{9.1}$$

The quantity g_n is related to the degeneracy of each species present, and is given by

$$g_n = 2 + (2)(2)\left(\frac{3}{4}\right) + (2)\left(\frac{3}{4}\right) N_\nu \tag{9.2}$$

where the first term is for photons (2 helicity states), the second term is for e^+/e^- (2 helicity states for each), and the last term is for neutrinos/antineutrinos (N_ν is the number of light flavors present). In the standard model we expect $N_\nu = 3$. The factor of 3/4 is the proper weighting for fermions relative to bosons (see Chapter 2).

9.1 Neutron/proton Ratio

The subsequent stages of nucleosynthesis in the early universe are governed by the relative number of neutrons and protons present (heavier nuclei without neutrons do not exist!). So our first goal is to understand and establish the neutron to proton ratio that results from the era of the Big Bang.

The total number density of nucleons is due to the process that created the excess of baryons at earlier times, and can only be inferred from observations of the present-day universe. However, the relative number of neutrons and protons is governed by the competing processes

$$\nu_e + n \;\leftrightarrow\; p + e^- \tag{9.3}$$

$$\bar{\nu}_e + p \;\leftrightarrow\; n + e^+ \,. \tag{9.4}$$

Since the nucleons are in thermal equilibrium with the leptons, the relative number of neutrons and protons is given by the ratio of Boltzmann factors (see Eq. 2.40)

$$\frac{n_n}{n_p} = \frac{e^{-\frac{M_n}{T}}}{e^{-\frac{M_p}{T}}} = e^{-\frac{Q}{T}} \tag{9.5}$$

where $Q = M_n - M_p = 1.293$ MeV. The processes (9.3, 9.4) are, at early times, rapid relative to the expansion rate of the universe. But as the universe cools, these processes become slower and the ratio of neutrons to protons freezes out. This occurs when the rate for neutron-proton conversion $\Gamma_{n\leftrightarrow p}$ falls below the expansion rate (given by Eq. 2.14), or

$$\Gamma_{n\leftrightarrow p} < \frac{\dot{R}}{R} \,. \tag{9.6}$$

The conversion rate $\Gamma_{n\leftrightarrow p}$ is governed by the weak interaction cross sections for the processes in (9.3) and (9.4). The cross section for

$$\bar{\nu}_e + p \to n + e^+ \tag{9.7}$$

can be computed using the methods used in Chapter 3 to compute the rate of neutron beta decay. At low energies (< 10 MeV), the same matrix elements as for the beta decay $n \to p\, e\, \bar{\nu}$ are responsible for the transition. To compute the cross section, we take the transition probability per unit time and divide by the incident flux (which for the relativistic neutrinos is c the speed of light):

$$d\sigma = \frac{d\omega}{c} = \frac{2\pi}{\hbar c}|H_{fi}|^2 \frac{dN}{dE_f} \,. \tag{9.8}$$

The density of final states is given by

$$\frac{dN}{dE_f} = \frac{d^3p_e}{(2\pi\hbar)^3} = \frac{p_e^2}{(2\pi\hbar)^3}\frac{dp_e}{dE_f} \cdot d\Omega \,. \tag{9.9}$$

We then integrate over the final β angle:

$$\sigma = \int \frac{d\sigma}{d\Omega} d\Omega = 4\pi \cdot \left[\frac{2\pi}{\hbar c}|H_{fi}|^2\right] \cdot \frac{p_e^2}{(2\pi\hbar)^3}\frac{dp_e}{dE_f} \,. \tag{9.10}$$

We neglect the recoil energy of the final nucleus: $dE_f \cong dE_e$ and we use $p_e\, dp_e = E_e\, dE_e$ to obtain the result

$$\sigma = \frac{1}{\pi\hbar^4}|H_{fi}|^2 \cdot p_e E_e \tag{9.11}$$

where

$$|H_{fi}|^2 = G_F^2\left[M_F^2 + g_A^2 M_{GT}^2\right] \tag{9.12}$$

$$= G_F^2\left[1 + 3g_A^2\right] \tag{9.13}$$

as in Eq. **??**. The final positron energy E_e is related to the incident $\bar{\nu}_e$ energy by

$$E_\nu = Q + E_e + T_n \tag{9.14}$$

$$\simeq Q + E_e \tag{9.15}$$

since at these energies the neutron recoil kinetic energy $T_n \sim 1$ keV is negligible relative to the other quantities. Recalling that $g_A \simeq 1.26$ and neglecting the electron mass we arrive at the approximate expression:

$$\sigma \simeq {G_F}^2 (E_\nu - Q)^2 \tag{9.16}$$

where we now use units with $\hbar = 1$. In the early universe the neutrinos are in thermal equilibrium at temperature T:

$$\sigma \sim G_F^2 (T - Q)^2 \,. \tag{9.17}$$

The rate $\Gamma_{n \leftrightarrow p}$ can be written

$$\Gamma_{n \leftrightarrow p} = n_\nu \langle \sigma v \rangle \tag{9.18}$$

where n_ν is the neutrino number density and $v (= c)$ the neutrino velocity. The number density of neutrinos is just

$$n_\nu = \frac{3}{4} \frac{\zeta(3)}{\pi^2} T^3 \tag{9.19}$$

and we find

$$\Gamma_{n \leftrightarrow p} \simeq G_F^2 T^3 (T - Q)^2 / 2 \,. \tag{9.20}$$

The actual value depends upon the neutron lifetime, which is required as input to obtain and accurate value for the quantity $M_F^2 + g_A^2 M_{GT}^2$.

Now using Eq. 2.14 and Eq. 2.4 we find

$$\frac{\dot{R}}{R} \simeq \sqrt{g_* G_N} T^2 \tag{9.21}$$

(here G_N is Newton's constant) and where we recall (see Chapter 2) that

$$g_* = 2 + (2)(2) \left(\frac{7}{8} \right) + (2) \left(\frac{7}{8} \right) \,. \tag{9.22}$$

We can now solve for the freeze-out temperature where

$$\Gamma_{n \leftrightarrow p} \sim \frac{\dot{R}}{R} \tag{9.23}$$

to obtain

$$T_f (T_f - Q)^2 \sim \frac{\sqrt{g_* G_N}}{G_F^2} \,. \tag{9.24}$$

Evaluating this expression yields an estimate for the freeze-out temperature of

$$T_f \sim 1 \text{ MeV} \,. \tag{9.25}$$

We can now use this value in Eq. 9.5 to obtain

$$\frac{n_n}{n_p} \simeq \frac{1}{6} \,. \tag{9.26}$$

(The actual value is sensitive to some details like N_ν, which makes the subsequent nucleosynthesis and final abundances of light elements also sensitive to this interesting quantity.) Finally, after the freeze-out some of the neutrons decay before the nuclear reactions associated with nucleosynthesis (that traps them in stable nuclei) occurs, and the actual value is given by

$$\frac{n_n}{n_p} \simeq \frac{1}{7} \,. \tag{9.27}$$

9.2 Production of Deuterium and Helium

The first step in the chain of nuclear reactions in the early universe is the capture of protons and neutrons to form deuterium

$$n + p \rightarrow d + \gamma(2.225 \text{ MeV}). \tag{9.28}$$

When the temperature is low enough that the high photon density is reduced sufficiently that the deuterons are stable ($T \sim 0.1$ MeV), further reactions can begin to take place. The next step is

$$p + d \rightarrow {}^3\text{He} + \gamma(7 \text{ MeV}) \tag{9.29}$$

followed by

$$p + {}^3\text{He} \rightarrow {}^4\text{He} + \gamma(20 \text{ MeV}). \tag{9.30}$$

The end product of this chain of reactions, ^{4}He, is very stable and so very little of it is processed further. In fact, essentially all of the neutrons end up in ^{4}He. The cross sections for proton capture on deuterium and ^{3}He are quite high and so the rates are fast compared to the expansion rate. In addition, the high photon energies required for the inverse reactions prohibit the photodisintegration reactions so, effectively, at these low temperatures only single captures are important. In the end, only a small number of d and ^{3}He remain when all the neutrons are captured and essentially all of them are in ^{4}He. Thus, the fractional abundance of ^{4}He is given simply by the neutron-proton ratio Eq. 9.27. One obtains the result for the mass fraction of ^{4}He, designated Y_p,

$$Y_p \equiv \frac{4n_{\text{He}}}{n_{\text{H}} + 4n_{\text{He}}} \tag{9.31}$$

$$= \frac{2\left(\frac{n_n}{n_p}\right)}{1 + \frac{n_n}{n_p}} \tag{9.32}$$

$$\simeq \frac{2/7}{8/7} = 0.25\,. \tag{9.33}$$

The actual value depends mildly upon η, the baryon to photon ratio, but this is a actually a reasonably good estimate. The best observational data to date indicate that the primordial value of $Y_p = 0.249 \pm 0.009$, in excellent agreement with the calculations. This is a very impressive and robust prediction of Big Bang Nucleosynthesis, and is a major cornerstone in modern cosmology.

The residual amounts of d and ^{3}He are rather small $\sim 10^{-5}$ as they are efficiently converted to ^{4}He. The actual amount is quite sensitive to the expansion rate, the nuclear reaction rates, and the temperature, but can be reliably computed during the phase until the endpoint of ^{4}He production. The predicted values for these abundances are very sensitive to the η, the baryon to photon ratio and are shown in Fig. 9.1.

9.3 Relic Neutrinos

The era of Big Bang Nucleosynthesis marks the point in the history of the universe where the weak interactions between neutrinos and baryons terminate, and the neutrinos are thereafter decoupled. At this point, we have a relativistic Fermi gas of neutrinos, three flavors, with a total density given by

$$n_\nu = 3\frac{3}{4}\frac{\zeta(3)}{\pi^2}T^3\,. \tag{9.34}$$

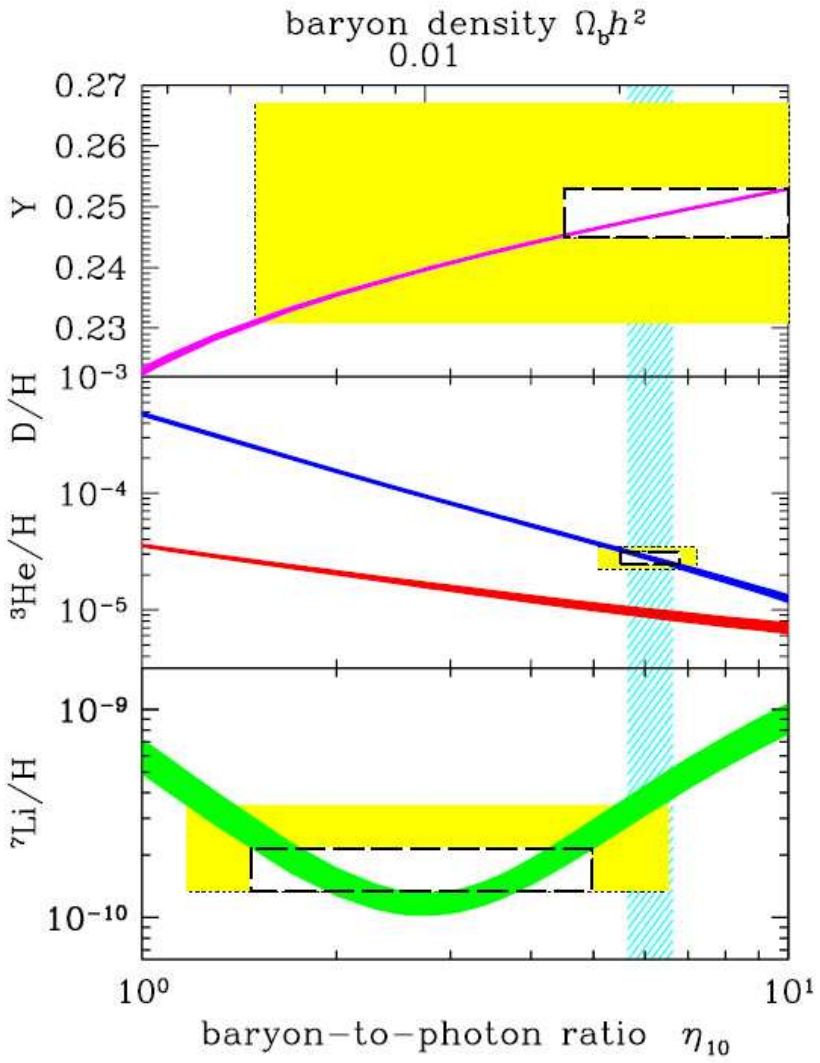

Figure 9.1: The relative abundances of d, ^{3}He, ^{4}He and ^{7}Li are shown as a function of the baryon to photon ratio $\eta_{10} = \eta \times 10^{10}$. The measured values from astronomical observations are shown as horizontal bands (1σ and 2σ). The curves are the predictions from BBN nucleosynthesis (width is the estimated uncertainty) and the vertical band at $\eta_{10} \simeq 6$ is the value extracted from fits of measurements of the cosmic microwave background.

The subsequent evolution of this sea of neutrinos is simply governed by the expansion of the universe. Shortly after the decoupling of the neutrinos (at $T \sim 1$ MeV) the photons are reheated by the annihilation of positrons. This reheating is isentropic, so the entropy given by Eq. 2.7 is conserved. Before reheating, we have

$$s = \frac{2}{3} g_*^0 \left(T^0\right)^3 \tag{9.35}$$

with $g_*^0 = 2 + 7/2$ corresponding to the photons and $e^\pm$ (the neutrinos are decoupled). Afterward, we have

$$s = \frac{2}{3} g_* T^3 \tag{9.36}$$

with $g_* = 2$. Therefore we find that the ratio of final to initial temperatures are

$$\left(\frac{T}{T^0}\right) = \left(\frac{g_*^0}{g_*}\right)^{1/3} \tag{9.37}$$

Thus the density of photons increases as

$$\begin{aligned} \frac{n_\gamma}{n_\gamma^0} &= \left(\frac{T}{T^0}\right)^3 && (9.38)\\ &= \left(\frac{g_*^0}{g_*}\right) && (9.39)\\ &= \left(1 + \frac{7}{4}\right) = \frac{11}{4}\,. && (9.40) \end{aligned}$$

Following this reheating, the photons and neutrinos both evolve based on the expansion of the universe. The ratios of temperatures T_ν/T_γ and the number densities n_ν/n_γ remain constant. At present, measurements of the cosmic microwave background yield the values $T_\gamma = 2.725$ K and $n_\gamma = 410.4\text{cm}^{-3}$. Thus, if the neutrinos have light enough masses (i.e., $m_\mu \ll T_\nu$) we would predict for the neutrinos today:

$$T_\nu = \left(\frac{4}{11}\right)^{1/3} T_\gamma = 1.95 \text{ K} \tag{9.41}$$

and a total number density

$$n_\nu = 3\frac{3}{4}(\frac{4}{11} n_\gamma) = 336 \text{ cm}^{-3} \tag{9.42}$$

where we have accounted for antineutrinos as well as neutrinos with only one helicity state each.

The neutrino masses are known to be light, less than about 1 eV, but are not zero. Through measurements of neutrino oscillations, the mass differences

$$\begin{aligned} \Delta m_{23}^2 &\simeq 3 \times 10^{-3} \text{ eV}^2 && (9.43)\\ \Delta m_{12}^2 &\simeq 7 \times 10^{-5} \text{ eV}^2 && (9.44) \end{aligned}$$

have been determined. Given the current neutrino temperature $T_\nu = 1.7 \times 10^{-4}$ eV, at least two of the neutrino states are non-relativistic (i.e., $\sqrt{\Delta m_{23}^2} > \sqrt{\Delta m_{12}^2} > T_\nu$). With at least one neutrino

mass (the heaviest $= m_h$) $m_h > \sqrt{\Delta m^2_{23}} \simeq 0.05$ eV we obtain a lower limit on the energy density of the neutrinos

$$\begin{aligned} \Omega_\nu &> \frac{n_\nu}{3} m_h && (9.45) \\ &> 6 \text{ eV/cm}^{-3} && (9.46) \\ &> 10^{-3}\Omega_0 && (9.47) \end{aligned}$$

where Ω_0 is the total energy density of the universe. The present experimental upper limit on the mass of the $\bar{\nu}_e$ is 3 eV. With the small mass differences implied by Eq. 9.43 and Eq. 9.44 it is possible that all three neutrinos have a mass of ~ 3 eV, which implies the upper bound

$$\Omega_\nu < 0.2\Omega_0 \, . \tag{9.48}$$

This is the largest possible value based on direct experimental data on neutrino masses. An indirect limit on the neutrino density has been obtained by recent analyses of the cosmic microwave background measurements using the WMAP satellite data:

$$\Omega_\nu < 0.015\Omega_0 \, . \tag{9.49}$$

Thus it appears that the neutrino contribution to the energy of the universe is somewhat less than the baryonic matter ($\Omega_b = 0.044\Omega_0$), but is likely at least comparable to the visible luminous matter in stars ($\Omega_{\rm lum} = 0.005\Omega_0$).

Chapter 10

The Power and Evolution of Stars

It is now well-established that fusion reactions provide the energy to make stars like the sun shine. The sun is a typical "main-sequence" star that is about 5 billion years old. In this chapter we will study the nuclear processes that power the energy output of the sun as a prototypical main-sequence star.

The sun is essentially a ball of 1.2×10^{57} hydrogen atoms, compressed by their mutual gravitational attraction, with a total mass of $M_\odot = 1.98 \times 10^{30}$ kg. The solar radius is $R_\odot = 6.96 \times 10^8$ m, implying an average density of 1.4 g/cm^3, but it is not constant and the density at the center of the sun is about 150 g/cm^3. The energy output (solar luminosity), in the form of thermal radiation, is $L_\odot = 3.8 \times 10^{26}$ Watts $= 2.4 \times 10^{39}$ MeV/s.

The gravitational compression heats the solar interior, but it is easy to demonstrate that this gravitational energy is insufficient to power the solar luminosity. Thus, we require another source of energy to make the sun shine so brightly for so long. The basic process that starts this process is a weak interaction, the fusion of two protons into a deuteron:

$$p + p \rightarrow d + e^+ + \nu \, . \tag{10.1}$$

The fact that this is a weak interaction makes the cross section very small at the energies provided by the interior solar temperature ($\sim 1.5 \times 10^7$ K). The energy produced in this reaction is

$$2M_p - M_d - m_e = 0.420 \text{ MeV} \tag{10.2}$$

and is primarily shared between the positron and neutrino in the final state. The neutrino escapes from the sun, but the positron's energy (including its rest mass) becomes part of the thermal energy produced by nuclear reactions in the solar interior.

The subsequent nuclear reactions involving deuterium and ^{3}He actually provide more energy, but this reaction governs the rate of "hydrogen burning" in the sun. At the central temperature and density of the sun, this $p-p$ fusion reaction has a mean time constant of 1.4×10^{10} years. This is essentially the reason that the sun can shine steadily for billions of years.

10.1 Nuclear Fusion

The fusion of charged particles at low energy is the dominant nuclear process occurring in stars like the sun. Here we consider the fusion of two nuclei with atomic numbers Z_1 and Z_2, separated

by a distance r. For $r > R_1$, the strong interaction potential between the nuclei can be neglected and the potential is just the coulomb potential $V_C(r) = Z_1 Z_2 e^2/r$. For light nuclei ($A < 16$) the radius $R_1 \sim 1-2$ fm, and the coulomb barrier is $E_C = V_C(R_1) > 1$ MeV. This is large compared to the typical kinetic energy $kT \sim 1$ keV. Thus the cross section for fusion is suppressed by the huge potential barrier that must be penetrated for the nuclear potential to take effect (i.e., where the nuclei overlap). In addition, one generally finds the condition for quasi-classical behavior is easily fulfilled:

$$\eta \equiv \frac{Z_1 Z_2 e^2}{\hbar v} \gg 1 \tag{10.3}$$

where v is the relative velocity of the nuclei. In this case, one can use the WKB approximation to compute the penetration through the barrier:

$$P_l \simeq \exp\left[-\frac{2\sqrt{2\mu}}{\hbar}\int_{R_1}^{R_2}\left[V_l(r) - E\right]^{1/2} dr\right] \tag{10.4}$$

in which μ is the reduced mass, R_2 is the classical turning point $[V_l(R_2) = E]$ and we have defined

$$V_l(r) \equiv V_C(r) + \frac{l(l+1)\hbar^2}{2\mu r^2}\,. \tag{10.5}$$

At very low energies, one can usually neglect $l > 0$ and keep only the $s-$ wave, and the exponent in Eq. 10.4 can be evaluated in the limit $E << E_C$ as

$$\frac{2\sqrt{2\mu}}{\hbar}\int_{R_1}^{R_2}\left[V_l(r) - E\right]^{1/2} dr = \frac{2\pi Z_1 Z_2 e^2}{\hbar v} \equiv 2\pi\eta\,. \tag{10.6}$$

The $s-$wave cross section for the nuclear fusion reaction can generally be written as

$$\sigma \simeq \frac{\pi}{k^2} P_0 \tag{10.7}$$

where $\hbar k$ is the momentum in the center of mass frame. Thus we expect the low energy cross section to depend on energy as

$$\sigma = \frac{S(E)}{E} e^{-2\pi\eta} \tag{10.8}$$

where $S(E)$ is expected to be a slowly varying function of E (for the case where there are no resonances at low energies). S is known as the astrophysical $S-$factor, and is the quantity that is usually calculated and compared to experimental data through the inverse of Eq. 10.8.

For the $p-p$ fusion reaction Eq. 10.1 the $S-$factor is given by $S_{11}(0) = 4 \times 10^{-22}$ keV-barns, which at the central solar temperature implies a tiny average cross section of

$$\langle\sigma_{pp}\rangle \simeq 4 \times 10^{-51}\ \mathrm{cm}^2\,. \tag{10.9}$$

The fact that Eq. 10.1 is a weak process, along with the coulomb penetration factor, combine to produce this very small cross section that implies the sun will shine for billions of years.

Following the process 10.1, the deuteron that is formed can readily fuse with another proton to form ^{3}He:

$$p + d \rightarrow {}^3\mathrm{He} + \gamma\,. \tag{10.10}$$

The $S-$factor for this process, S_{12} is much larger than S_{11}

$$S_{12} \simeq 2.5 \times 10^{-4} \text{ keV} - \text{b} \,. \tag{10.11}$$

Thus the deuterons produced in Eq. 10.1 only last a few seconds after they are created. Therefore a significant concentration of deuterium does not build up, but instead there is a growth in the concentration of ^{3}He.

In the final step of the $p-p$ chain of reaction, two ^{3}He will fuse to form ^{4}He:

$$^3\text{He} + {}^3\text{He} \rightarrow {}^4\text{He} + 2p \,. \tag{10.12}$$

This reaction has a healthy $S-$factor, given by

$$S_{33} \simeq 5.3 \text{ MeV} - \text{b} \tag{10.13}$$

but the higher coulomb barrier penetration and lower concentration of ^{3}He moderates the rate of this reaction. The result is that ^{3}He reacts on time scale of order a million years in the center of the sun.

While other small branches contribute, this is the major reaction chain that converts protons into the tightly bound ^{4}He. The positrons produced in the initial p-p fusion reactions annihilate with electrons into photons ($e^+ + e^- \rightarrow 2\gamma$) so actually the complete sequence converts 4 protons and 2 electrons into ^{4}He, 2 ν's and electromagnetic energy (that eventually leads to the thermal energy associated with "sunshine"):

$$2e^- + 4p \rightarrow {}^4\text{He} + 2\nu \,. \tag{10.14}$$

The total energy released in this chain of reactions is

$$E_{\text{release}} = 4M_H - M(^4\text{He}) - 2\langle E_\nu \rangle \tag{10.15}$$

$$= 26.7\,\text{MeV} \tag{10.16}$$

where M_H and $M(^4\text{He})$ are the *atomic* masses (including electrons) of Hydrogen and ^{4}He.

The energy released, E_{release} can be combined with the solar luminosity $L_\odot = 3.83 \times 10^{33}$ ergs/sec to calculate the expected production rate of p-p neutrinos to be 1.8×10^{38} sec^{-1} which yields a flux at the earth of

$$\phi_{pp} = 6.4 \times 10^{10}\,\text{cm}^{-2}\text{s}^{-1} \,. \tag{10.17}$$

This is an extremely important result, and follows only from assuming the p-p chain reactions, energy conservation, and the solar luminosity. More detailed calculations that take into account other small contributions to the solar luminosity predict

$$\phi_{pp} = 6.00 \times 10^{10}\,\text{cm}^{-2}\text{s}^{-1} \,. \tag{10.18}$$

A star like the sun will burn hydrogen for billions of years, converting the protons into ^{4}He. There is no stable nucleus with $A = 5$, so there is no opportunity for the ^{4}He to capture a proton and thus the star will steadily increase its concentration of ^{4}He. A dense core of ^{4}He forms, contracting and increasing in temperature driven by the increased gravitational binding. Outside this core is hydrogen which is heated by the ^{4}He core. Hydrogen burning continues at the surface of the ^{4}He core, heating the hydrogen envelope so that it greatly expands. A star like the sun will expand its radius to about 200 times the current solar radius when it reaches this "red giant" phase. When the hydrogen fuel is exhausted, a star like the sun becomes a ball of gradually cooling ^{4}He. Actually, some of the ^{4}He is processed in helium burning, a process that is more important for heavier stars with $M > 3M_\odot$.

10.2 Helium burning

Although it is possible to fuse ^{4}He and ^{3}He, the concentration of ^{3}He is never sufficient to burn a significant fraction of the ^{4}He. Of course one could fuse two α particles, but the resulting nucleus ^{8}Be is not stable and quickly ($\sim 10^{-16}$ sec) decays back to two α particles. Nucleosynthesis beyond ^{4}He actually proceeds by another route: the triple α reaction. In this process, the unstable ^{8}Be can capture another α to form ^{12}C in an excited state. By an amazing coincidence (see Fig. 10.1), ^{12}C has an excited state at 7.654 MeV that lies just (287 keV) above the energy of ^{8}Be + α. This resonance is essential to increase the cross section in order for the 3α process to occur at a sufficient rate. (Were it not for this resonance, the abundance of carbon, oxygen and heavier elements in the universe would be greatly reduced to the point where we would not likely exist.) When the temperature rises above $\sim 10^8$ K, the He core of a star can ignite this reaction. It turns out that only relatively massive stars with $M > 3M_\odot$ have a hot enough He core to ignite helium burning.

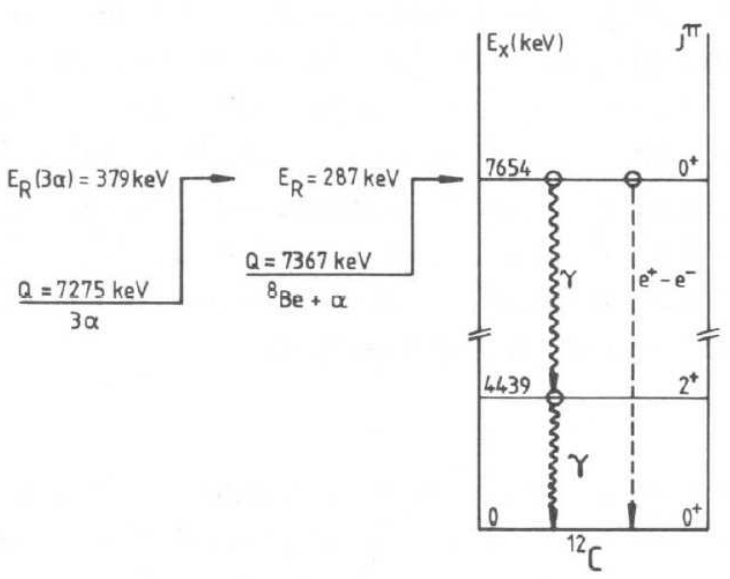

Figure 10.1: Energy level diagram showing the relevant states in ^{12}C for the 3α reaction.

The carbon collects in the center of the star, forming a carbon core inside the ^{4}He. At the surface of the carbon core, the final helium burning process occurs:

$$^{12}\mathrm{C} + \alpha \rightarrow {}^{16}\mathrm{O} + \gamma\,. \tag{10.19}$$

If the star is not massive enough, the helium burning left behind a star with mostly carbon and oxygen nuclei. The further gravitational contraction will be balanced by the degenerate electron pressure which we turned to now.

10.3 White Dwarf Star

Stars with $M < 9M_\odot$ will shed their hydrogen envelopes when the core reaches about $1M_\odot$, which then ultimately collapses to form a white dwarf, with a typical radius similar to that of the earth:

6000 km. The white dwarf is a star that is stabilized against further collapse by the degeneracy pressure of the Fermi gas of electrons. Further thermonuclear reactions are not significant and nucleosynthesis is essentially terminated.

To understand the role of the degenerate electron pressure, we begin by considering a mature (one that is approaching the limit of its available thermonuclear fuel) star composed of atoms each with mass number A. Let there be a total of n nucleons so the number of atoms is $\frac{n}{A}$. We define the proton fraction $x \equiv \frac{Z}{A}$ so that the total number of electrons is $n_e = xn$ (the star is electrically neutral). After exhausting its thermonuclear fuel the gravitational force exceeds the thermal pressure associated with thermonuclear reactions, and the radius contracts to the point where the density is very high and atoms lose identity. Then the e^- form a Fermi gas and the density is high enough that the pressure of the Fermi gas (Pauli principle) is the main support against further collapse. This is a "white dwarf" star.

Assuming the temperature is not so high that the non-relativistic approximation is valid for the electron gas. The degenerate e^- gas has the properties:

$$n_e = \frac{\Omega}{3\pi^2}k_f^3 \tag{10.20}$$

$$\langle T\rangle = \frac{3}{5}\frac{\hbar^2 k_f^2}{2m_e} = \frac{3\hbar^2}{10m_e}\left(\frac{3\pi^2 n_e}{\Omega}\right)^{2/3} \tag{10.21}$$

$$\Omega = \frac{4\pi}{3}r^3, \quad n_e = xn \tag{10.22}$$

so the total kinetic energy is

$$\langle T\rangle = \frac{3\hbar^2}{10m_e r^2}\left(\frac{9\pi xn}{4}\right)^{2/3} \tag{10.23}$$

The total energy of the star is the sum of the total e^- kinetic energy and the gravitational potential energy. For a uniform sphere, the gravitational potential is

$$-\frac{3}{5}G\frac{M^2}{r} \tag{10.24}$$

so we have

$$E(r) = \frac{3\hbar^2 xn}{10m_e r^2}\left(\frac{9\pi xn}{4}\right)^{2/3} - \frac{3}{5}\frac{Gn^2M_p^2}{r}\,. \tag{10.25}$$

(The assumption of a uniform sphere is clearly a rather crude approximation, but the results for a correct treatment are quantitatively very similar.) To find the equilibrium radius, we set the derivative of the energy with respect to the radius to zero

$$\left.\frac{dE(r)}{dr}\right|_{r_{eq}} = 0 \tag{10.26}$$

which yields the result

$$r_{eq} = \frac{\hbar^2 x}{GnM_p^2 m_e}\left(\frac{9\pi xn}{4}\right)^{2/3}\,. \tag{10.27}$$

For $M = M_\odot$ =1 solar mass= nM_p we find $n = 1.2 \times 10^{57}$. Now we assume equal numbers of protons and neutrons so that $x \cong \frac{1}{2}$ and use

$$\begin{aligned} G &= 1.32 \times 10^{-52} \text{ cm/GeV} && (10.28)\\ \hbar &= 1.973 \times 10^{-14} \text{ GeV} - \text{cm} && (10.29)\\ M_p &= 0.938 \text{ GeV} && (10.30)\\ m_e &= 5.11 \times 10^{-4} \text{ GeV} . && (10.31) \end{aligned}$$

The radius of the star is

$$\begin{aligned} r_{eq} &= 7.1 \times 10^8 \text{ cm } (\ll 7 \times 10^{10} \text{ cm} = R_\odot) && (10.32)\\ &\approx r_{\text{earth}}! && (10.33) \end{aligned}$$

The volume and density are then

$$\begin{aligned} \Omega &= 1.5 \times 10^{27} \text{ cm}^3 \\ n/\Omega &= 10^{30}/\text{cm}^3 . && (10.34) \end{aligned}$$

This is much greater than an inverse atomic volume (10^{24} cm^3), so that the atoms are totally overlapping and the electrons are not confined to individual atoms. [The average distance between atomic nuclei is about 10^3 fm = 10^{-2} A, much smaller than the size of an atom, but much larger than the nuclear size.] The mass density is

$$\begin{aligned} \rho &= 1.3 \times 10^6 \text{ g/cm}^3 && (10.35)\\ &= 1.3 \text{ tons/cm}^3 && (10.36)\\ &\ll \rho_{NM} \sim 10^{14} \text{ g/cm}^3 && (10.37) \end{aligned}$$

where ρ_{NM} is the mass density of normal nuclear matter. The average electron kinetic energy is $\langle T \rangle = 0.12$ MeV so we are still in the zero temperature limit but since $\langle T \rangle$ is not insignificant compared to m_e we are close to needing to consider the electrons as a relativistic Fermi gas. Thus, for masses beyond 1 $M_\odot$ we need relativistic e^-.

For ultra-relativistic electrons the Fermi energy and mean total energy are given by the expressions (neglecting now the electron mass)

$$\begin{aligned} E_f &= \hbar \left(\frac{3\pi^2 n_e}{\Omega} \right)^{1/3} && (10.38)\\ \langle E \rangle &= \frac{3}{4} E_f && (10.39) \end{aligned}$$

and we then find

$$\begin{aligned} E(r) &= \frac{3\hbar x n}{4r} \left(\frac{9\pi x n}{4} \right)^{1/3} - \frac{3}{5} G \frac{n^2 M_p^2}{r} && (10.40)\\ &\equiv \frac{\alpha n^{4/3} - \beta n^2}{r} . && (10.41) \end{aligned}$$

Therefore, if we increase n the numerator eventually becomes negative. Then $E(r)$ decreases (becomes more negative) as the radius r decreases and the star will collapse! Thus, there is a critical number $n_{\rm crit}$ corresponding to $E(r) = 0$.

$$n_{\rm crit}^{2/3} = \frac{5\hbar x}{4GM_p^2}\left(\frac{9\pi x}{4}\right)^{1/3} \tag{10.42}$$

$$n_{\rm crit} = \left(\frac{9\pi x}{4}\right)^{1/2}\cdot\left(\frac{5\hbar x}{4GM_p^2}\right)^{3/2} \tag{10.43}$$

$$= \left(\frac{9\pi}{4}\right)^{1/2}\cdot\left(\frac{5\hbar}{4GM_p^2}\right)^{3/2} x^2 \tag{10.44}$$

$$= \frac{3(125\pi)^{1/2}}{16}\cdot\left(\frac{\hbar}{GM_p^2}\right)^{3/2} x^2 \tag{10.45}$$

This is known as the "Chandrasekhar limit", and numerically

$$\left(\frac{\hbar}{GM_p^2}\right)^{3/2} = 2.2\times 10^{57} \tag{10.46}$$

and so the critical number is $n_{\rm crit} = 2.06\times 10^{57}$ corresponding to a total mass

$$n_{\rm crit} M_p = 1.7\ M_\odot\,. \tag{10.47}$$

The actual value, obtained by numerical solution to the equations that establish equilibrium as a function of radius and including the rest mass of electron, is $1.4M_\odot$.

10.4 Type Ia Supernova

Type Ia Supernova explosion is one of the spectacular optical events in the Universe. For this reason, Type Ia supernova has been regarded as a standard candle in measuring cosmological distances.

Type Ia supernova is believed to start from a binary system consisting of a white dwarf and an accompanying main sequence star. In the white dwarf, the helium has burned almost completely and resulting a core of carbon and oxygen below Chandrasekar limit. However, the white dwarf steadily accrete matter from its companion and eventually its mass exceeds the limit. Once this happens, the star will undergo gravitational collapse and release huge amount of gravitational energy in the form of heat which leads to nuclear reactions producing heavier elements such as iron, nickel and cobalt by burning carbon and oxygen. These energy produces a huge explosion which result in type Ia supernova, and the entire star is almost entirely destroyed in the process.

In the spectrum of light from type Ia supernova, there is no hydrogen line, because the hydrogen has been burned before the star collapse happens.

10.5 Fusion in Advanced Massive Stars

Heavier stars with $M > 9M_\odot$ can generate higher internal pressures and temperatures that are sufficient to ignite more advanced stages of nuclear burning and continue the process of nucleosynthesis. For these stars, the hydrogen burning phase is relatively short, only about 10 million

years, before beginning helium and then carbon burning. Once the carbon burning phase begins, the star has only a few thousand years left to complete the chain of rapid nucleosythesis reactions that produce heavier elements up to iron. As shown in a previous chapter, the binding energy per nucleon of stable nuclei increases with nuclear mass number A until $A = 56$, with ^{56}Fe being the most stable nucleus. Beyond ^{56}Fe it is not possible to form heavier nuclei by the fusion process.

Carbon burning proceeds when the temperature reaches $\sim 5 \times 10^8$ K and the central density exceeds 10^5 g/cm^3. The main reaction is

$$^{12}\mathrm{C} + {}^{12}\mathrm{C} \rightarrow {}^{24}\mathrm{Mg}^* \rightarrow {}^{20}\mathrm{Ne} + \alpha \, . \tag{10.48}$$

In addition, there are other reaction products and many reactions that involve capturing protons, alphas, neutrons, and beta decays also occur. Nuclei up to $A = 35$ are produced in significant quantities as a result of these reactions. But Ne and O are the most abundant products of carbon burning.

At higher temperatures (10^9 K $\sim$ 100 keV) and densities (10^6g/cm^3, the neon burning phase begins. Photodisintegration of Ne produces α particles via $\gamma + {}^{20}\mathrm{Ne} \rightarrow {}^{16}\mathrm{O} + \alpha$ and these α's can in turn be captured on ^{2}0Ne:

$$^{20}\mathrm{Ne} + \alpha \rightarrow {}^{24}\mathrm{Mg} + \gamma \, . \tag{10.49}$$

Neon burning is followed by oxygen burning, predominantly

$$^{16}\mathrm{O} + {}^{16}\mathrm{O} \rightarrow {}^{32}\mathrm{S}^* \rightarrow {}^{28}\mathrm{Si} + \alpha \tag{10.50}$$

which provides the fuel for silicon burning. Silicon burning involves a complex network of α, p, n, and γ induced reactions that generate nuclei all the way up to ^{56}Ni. The end result of this process is the collection of the most stable nucleus, ^{56}Fe, at the center of the star. The other burning processes continue in shells outside the Fe core. A calculation of the relative fractions of nuclides present as a function of interior mass is shown in Fig. 10.2. It can be seen that the star has an onion-like structure, with different well-defined regions corresponding to the different nuclear burning processes.

If the mass of a star is heavy, the iron core grows until it reaches about 1.4 $M_\odot$, where the degeneracy pressure of the electrons becomes insufficient to prevent further shrinking. The core will collapse, and the result is a type II supernova explosion. It is generally thought that the supernova explosion is the source of nuclear processes that produce all the elements heavier than iron. We will come to this topic later on.

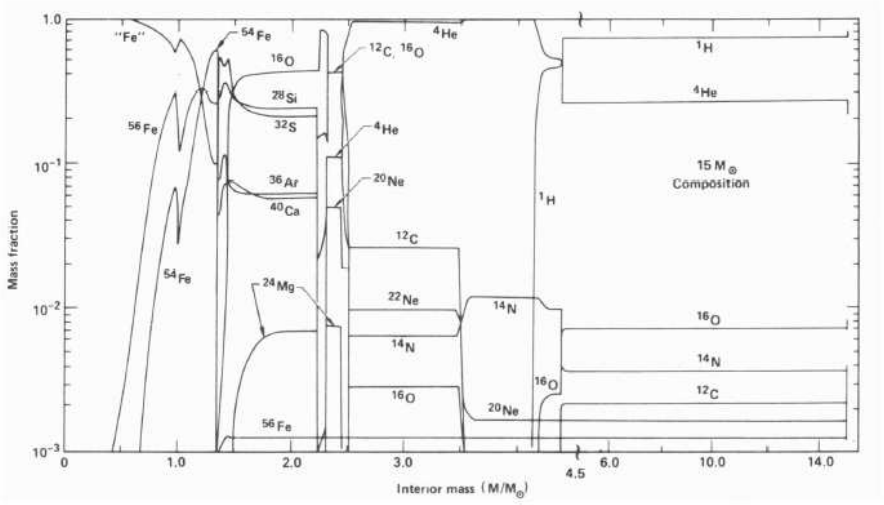

Figure 10.2: Mass fractions of nuclides as a function of interior mass (increasing with radius) for a 15 $M_\odot$ star at the end of nuclear burning just before the core collapses.

Chapter 11

Neutrinos and Neutrino Cosmology

The neutrino was originally invented in 1930 by Pauli to salvage conservation of energy and angular momentum in nuclear beta decay. At the time it was known that in the beta decay $^6\mathrm{He} \rightarrow {}^6\mathrm{Li} + e^-$ there were two problems:

- the measured spectrum of electron kinetic energy was a continuous distribution from zero to the maximum value expected from the difference in masses of ^{6}He and ^{6}Li,
- the spin of ^{6}He is $J_i = 0$ and the final ^{6}Li has spin $J_f = 1$, implying the electron should have integral angular momentum which is not possible for a fermion.

Thus Pauli had the idea to invent a new neutral fermion emitted with the electron, later known as the neutrino, that was not detected in the experiments. This would enable restoration of conservation of energy and angular momentum.

Due to its lack of electric charge and the weakness of its interactions, the neutrino went undetected for many decades. The neutrino was finally observed in experiments in the 1950's by Reines and Cowan. These experiments actually were able to detect the antineutrinos emitted by nuclear reactors via the inverse beta decay process $\bar{\nu}_e + p \rightarrow e^+ + n$.

In the latter half of the 20th century, many experiments were performed with muon-type neutrinos (ν_μ) produced in accelerator experiments through the decay of pions $\pi^+ \rightarrow \mu^+ + \nu_\mu$. These ν_μ (and also $\bar{\nu}_\mu$) were observed to only produce μ^- (or μ^+) in their interactions with matter. Thus they were quite distinct from the ν_e and $\bar{\nu}_e$ produced in nuclear beta decays. In addition, the discovery of the heavier τ lepton introduced another flavor of neutrino, ν_τ, which was eventually observed as well.

In 1968, Ray Davis and collaborators reported the first observation of neutrinos from the sun. Their experiment involved the use of 100,000 gallons of perchlorethylene (cleaning solution) located deep underground (to avoid cosmic rays) in a mine in South Dakota. The chlorine in the detector could be transformed into argon through the inverse beta process $\nu_e + {}^{37}\mathrm{Cl} \rightarrow {}^{37}\mathrm{Ar} + e-$, and the argon atoms could be extracted from the liquid and detected through their decay (^{37}Ar decays with half-life $t_{1/2} = 35$ days). Although Davis and collaborators reported the observation of a signal indicating the presence of solar neutrinos, the measured rate was more than a factor of 2 less than the predicted rate. Throughout the remainder of the 20th century, additional measurements of solar neutrinos of various energies all indicated a deficit of flux compared to the expected rates. The issue was finally resolved during the period 1998-2003 when it was established that neutrinos

have finite mass and that the flavor eigenstates are not the mass eigenstates. This enables the process known as neutrino oscillations, where the flavor states *oscillate* as the neutrino propagates through space.

The absolute scale of neutrino mass and the basic nature of the neutrino (whether it is its own antiparticle, i.e., Majorana type, or not i.e, Dirac type fermion) are still to be determined. Nuclei and their properties have been, and continue to be, an essential aspect of the study of neutrinos.

11.1 Nuclear Beta Decay

The process of nuclear beta decay is important both as a means of transforming nuclei into one another (in the laboratory and in the stars) and as a crucial means of testing the fundamental interaction responsible for it occurrence: the weak interaction. There are three basic processes (all related): 1.) electron (β^- decay, 2.) positron (β^+) decay, and 3.) atomic electron capture. We first consider the definitions of these processes and the energetics associated with each of them.

Electron (β^-) decay

This process involves the transformation of a nucleus (Z, N) into $(Z+1, N-1)$ through the emission of an electron ("β- particle") and an anti-neutrino (electron-type) $\bar{\nu}_e$:

$$(Z, N) \rightarrow (Z + 1, N - 1) + e^- + \bar{\nu}_e \, . \tag{11.1}$$

The energy released in the process is shared between the e^- and $\bar{\nu}_e$ is known as the "Q value"$\equiv Q$. (A small amount of kinetic energy goes into the recoiling $(Z+1, N-1)$ nucleus, but we will generally neglect it.)

The simplest example of nuclear beta decay is the decay of the free neutron:

$$n \rightarrow p + e^- + \bar{\nu}_e \, . \tag{11.2}$$

The energy released is

$$Q = M_n - M_p - m_e - m_\nu \, . \tag{11.3}$$

We will see later that we know the neutrino is massless or very light so we may take $m_\nu \simeq 0$, and thus

$$\begin{aligned} Q = M_n - M_p - m_e &= (939.57 - 938.28 - 0.51)\,\text{MeV} & (11.4) \\ &= 0.78\,\text{MeV}. & (11.5) \end{aligned}$$

Since the energy is shared between the e^- and $\bar{\nu}_e$, the maximum kinetic energy of the e^- is $Q = 0.78$ MeV.

More generally, for $(Z, N) \rightarrow (Z + 1, N - 1) + e^- + \bar{\nu}_e$ we define $M(Z, N) \equiv$ atomic mass (including Z electrons) and then

$$Q_{\beta^-} = M(Z, N) - M(Z + 1, N - 1) \, . \tag{11.6}$$

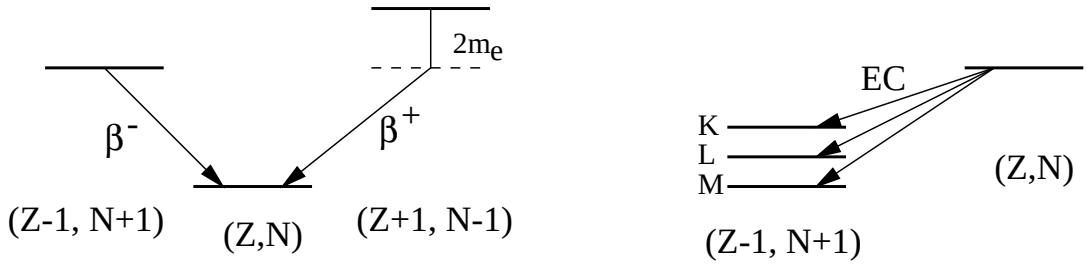

Energy Diagrams for β^- , β^+ , and EC Processes

Figure 11.1: Energy diagrams for electron, positron and electron capture processes.

Positron decay

Positron or β^+ decay is the process

$$(Z, N) \rightarrow (Z - 1, N + 1) + e^+ + \nu_e \tag{11.7}$$

and the Q-value is given by the expression

$$Q_{\beta^+} = M(Z, N) - M(Z - 1, N + 1) - 2m_e \tag{11.8}$$

(note that we have used $m_{e^+} = m_{e^-}$).

Electron capture (EC)

A process very closely related to β^+ decay is atomic electron capture:

$$(Z, N) + e^- \rightarrow (Z - 1, N + 1)^* + \nu_e$$

which involves the emission of a monoenergetic neutrino and generally leaves the residual $(Z - 1, N + 1)^*$ atom in an excited electronic state. The captured electron is usually in the innermost s-state ("K-shell") since this electron has the greatest overlap with the initial nucleus. The energetics of this process is given by

$$Q_{EC} = M(Z, N) - M(Z - 1, N + 1) - B_{e^-} \tag{11.9}$$

where B_{e^-} is the binding energy of e^- hole.

Theory of Nuclear Beta Decay

Nuclear beta (β^- or β^+) proceeds via the weak interaction, and thus we may use first order perturbation theory as an excellent approximation. Thus we utilize Fermi's golden rule and write

$$d\omega = \frac{2\pi}{\hbar} |H_{fi}|^2 \frac{dn}{dE_f} \tag{11.10}$$

where the density of final states may be written

$$\frac{dn}{dE_f} = \frac{d^3p_e}{(2\pi\hbar)^3} \cdot \frac{d^3p_\nu}{(2\pi\hbar)^3} \cdot \delta(E_0 - E_e - E_\nu) \tag{11.11}$$

where $E_0 \equiv Q + m_e$ = maximum total β energy E_e.

We also will assume the long wavelength limit, since generally the lepton momenta p_e and p_ν are both less than 10 MeV so that the wavelength of the lepton is

$$\lambda = \frac{2\pi\hbar}{p} \gtrsim 100 \text{ fm} \tag{11.12}$$

which is much greater than the nuclear radius. Therefore, H_{fi} will be independent of p_e and p_ν but may depend on the angle

$$\cos\theta_{e\nu} = \frac{\vec{p}_e \cdot \vec{p}_\nu}{p_e p_\nu} \,. \tag{11.13}$$

Since we won't detect the e^- direction, nor the ν (direction or energy) we will integrate over the e^-, ν angles (note that $p_\nu = E_\nu$ for $m_\nu = 0$):

$$d\omega = \frac{2\pi}{\hbar} \int \frac{1}{(2\pi^2\hbar^3)^2} |M_{fi}|^2 p_e^2 dp_e p_\nu^2 dp_\nu \delta(E_0 - E_e - E_\nu) \tag{11.14}$$

$$= \frac{1}{2\pi^3\hbar^7} |M_{fi}|^2 (E_0 - E_e)^2 p_e^2 dp_e \,. \tag{11.15}$$

Allowing for the Coulomb effect on e^- will modify the density of final states, and this has the effect that we must multiply our result by $F(Z, E_e) \equiv$ "Fermi Function". In the absence of the Coulomb interaction on the final e^-, $F(Z = 0, E_e) = 1$. Finally, we use that $p_e dp_e = E_e dE_e$ to obtain

$$d\omega = \frac{1}{2\pi^3\hbar^7} |M_{fi}|^2 F(Z,\ E_{e^-}) (E_0 - E)^2 p_e E_e dE_e \tag{11.16}$$

Beta energy spectrum

The spectrum of beta energies is then given by $\frac{d\omega}{dE_e}$, and since $|M_{fi}|^2$ is independent of the electron energy we have a relatively simple expression for the electron energy spectrum. If we define

$$K(E_e) \equiv \left[\frac{d\omega/dE_e}{F(Z, E_e) p_e E_e} \right]^{1/2} \tag{11.17}$$

(known as a "Kurie plot") we expect a linear function that intercepts the energy axis at the "endpoint" energy E_0. This is a very useful method for experimentally measuring E_0 and therefore Q which can then be used to determine masses of nuclei.

In addition, the effect of a finite $m_\nu \neq 0$ is to cause a distortion of the spectrum in the region near $E = E_0$:

$$d\omega = \frac{1}{2\pi^3\hbar^7} |M_{fi}|^2 F(Z,\ E_e) p_e E_e (E_0 - E_e)^2 \sqrt{1 - \frac{m_\nu^2}{(E_0 - E_e)^2}} \cdot dE_e \,.$$

The best direct information on the electron neutrino mass comes from measurements of Kurie plots near the endpoint in the beta decay of tritium. The favorable conditions of this decay include

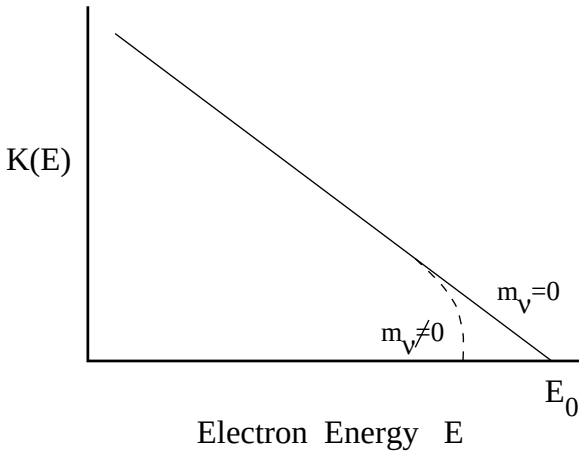

Figure 11.2: Kurie plot of the beta decay spectrum showing the effect of finite neutrino mass.

- • Small $Z = 1$ [F distortion minimal]
- • E_0 small [$Q = 18.6$ keV!]

The results of the most recent measurements yield an upper limit $m_\nu < 3$ eV, and further higher precision measurements are planned. This is one of the most promising methods to establish the absolute scale of the neutrino mass.

Nuclear Matrix Elements ("allowed" transitions)

We have previously studied the beta decay of the neutron in Chapter 3. There we introduced the "Fermi" (M_F) and "Gamow-Teller" (M_{GT}) matrix elements. For complex nuclei, we can generalize the definition as follows:

$$|M_{fi}|^2 = G^2 \left[M_F^2 + g_A^2 M_{GT}^2 \right] \tag{11.18}$$

$$M_F = \langle f|T^+|i\rangle; \quad (T^+ \equiv \sum_k \tau_k^+) \tag{11.19}$$

$$M_{GT} = \frac{1}{\sqrt{2J_i+1}} \langle f \| \sum_k \tau_k^+ \sigma_k \| i \rangle \, . \tag{11.20}$$

These operators imply that there are selection rules for nuclear beta decay. The Fermi matrix element is a scalar under rotations and does not change parity. Thus for Fermi (F) transitions we must have no change in angular momentum ($\Delta J = 0$ or $J_f = J_i$) and no parity change ($\Delta\pi = 0$ or $\pi_f = \pi_i$). These transitions only occur between states of an isotopic multiplet, connected by the isospin raising operator T^+. For Gamow-Teller (GT) transitions, the operator is a vector under rotations and also there is no parity change ($\Delta J = 0, 1$ or $J_f = J_i \pm 1$, and $\Delta\pi = 0$). If $J_i \neq 0$ then one could also have $J_f = J_i$ for GT transitions. These selection rules for F and GT decays together define the class of decays known as "allowed" transitions. The typical decay scheme is shown in Figure 11.3.

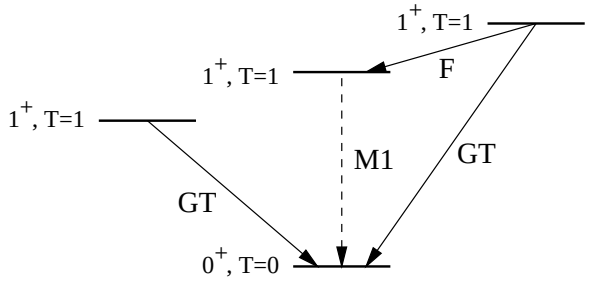

Typical Scheme of Fermi (F) and Gamow-Teller (GT) Decays

Figure 11.3: Typical decay scheme involving β^- and β^+ decays.

Classification of β-Decay Transitions

If we kept higher order terms (from expanding $e^{i\vec{p}_e\cdot\vec{r}_e}$) then there are other possibilities associated with higher multipoles. These are suppressed in strength relative to the "allowed" transitions for the same reason that higher order multipoles are suppressed in γ decays, i.e., we are in the long wavelength approximation and $p_eR \ll 1$. Decays that do not obey the "allowed" transition selection rule are thus called "forbidden" transitions.

Nuclear beta decays are classified according the the change in nuclear angular momentum and parity.

$$\vec{J}_i = \vec{J}_f + \vec{L}_\beta + \vec{S}_\beta \tag{11.21}$$

where $\vec{J}_{i,f}$ initial and final nuclear angular momenta and L_β and S_β are the orbital and spin angular momenta of the beta-neutrino combination. are the The parity eigenvalues of the initial and final nuclear states are given by

$$\pi_i = \pi_f \cdot (-1)^{L_\beta} \ . \tag{11.22}$$

For the spin angular momentum, there are 2 types of decay:

Fermi transitions	$\vec{S}_\beta = \vec{0}$
Gamow-Teller transitions	$\vec{S}_\beta = \vec{1}$

For each of these there are allowed and forbidden decays:

Allowed transitions	$\vec{L}_\beta = \vec{0}$
1st forbidden transitions	$\vec{L}_\beta = \vec{1}$
2nd forbidden transitions	$\vec{L}_\beta = \vec{2}$

Allowed transitions

These decays have $\vec{L}_\beta = 0$. $\pi_i = \pi_f$ and their properties are summarized in Table 11.1.

Fermi-type ($\vec{S}_\beta = \vec{0}$)	Gamow-Teller type $\vec{S}_\beta = \vec{1}$
$\vec{J}_i = \vec{J}_f$	$\vec{J}_i = \vec{J}_f + \vec{1}$
$\|\Delta J\| = 0$	$\|\Delta J\| = 0,\ 1:$ no $0^+ \to 0^+$
$0^+ \to 0^+$: superallowed	$0^+ \to 1^+$: unique Gamow-Teller

Table 11.1: Properties of allowed beta transitions.

1st forbidden transitions

These decays have $\vec{L}_\beta = \vec{1},\ \pi_i = -\pi_f$ and the properties listed in Table 11.2.

Fermi-type ($\vec{S}_\beta = \vec{0}$)	Gamow-Teller type ($\vec{S}_\beta = \vec{1}$)	
$\vec{J}_i = \vec{J}_f + \vec{1}$	$\vec{J}_i = \vec{J}_f + \underbrace{\vec{1} + \vec{1}}_{\vec{0},\ \vec{1},\ \vec{2}}$	
$\|\Delta J\| = 0,\ 1$	3 types:	
no $0^- \to 0^+$	(i) $\|\Delta J\| = 0$	
	(ii)$\|\Delta J\| = 0,\ 1;$	no $0^- \to 0^+$
	(iii) $\|\Delta J\| = 0,\ 1,\ 2;$	no $0^- \to 0^+$
		no $1^+ \to 0^-$
		no $\frac{1}{2}^+ \to \frac{1}{2}^-$

Table 11.2: Properties of first forbidden beta transitions.

Decay Rates

We may now compute the total decay rate (integrate over dE_e) to obtain

$$\omega = \frac{|M_{fi}|^2 m_e^5}{2\pi^3 \hbar^7} \frac{1}{m_e^5} \int_{m_e}^{E_0} F(Z,\ E)\ (E_0 - E)^2 pE dE\,. \tag{11.23}$$

We then define the Fermi Integral

$$f(E_0, Z) \equiv \frac{1}{m_e^5} \int_{m_e}^{E_0} F(Z,\ E)\ (E_0 - E)^2 pE dE \tag{11.24}$$

which are standard tabulated functions. In the limit $Z \to 0,\ m_e \ll E_0$ we can use the simple approximation

$$f = \frac{1}{m_e^5} \int_0^{E_0} E^2 (E_0 - E)^2 dE = \frac{E_0^5}{30\, m_e^5} \tag{11.25}$$

Therefore, we roughly expect $\omega \propto E_0^5$ and the decay rate is a rather strong function of the available energy.

The decay rate is related to the half-life $t_{1/2}$ by

$$\omega = \frac{\ln 2}{t_{1/2}} = \frac{|M_{fi}|^2 m_e^5 f}{2\pi^3 \hbar^7} \tag{11.26}$$

and it is customary to define the "comparative half-life" or "$ft_{1/2}$-value" as

$$ft_{1/2} \equiv \frac{2\pi^3 \hbar^7 \ln 2}{|M_{fi}|^2 m_e^5} \,. \tag{11.27}$$

This comparative half-life is related to simple matrix elements and fundamental constants only:

$$ft_{1/2} = \frac{2\pi^3 \hbar^7 \ln 2}{G^2 m_e^5 \left[M_F^2 + g_A^2 M_{GT}^2\right]} = \frac{6221 \text{ sec}}{M_F^2 + g_A^2 M_{GT}^2} \,. \tag{11.28}$$

As a common example, we consider a $0^+(T=1, M_T=-1) \to 0^+(T=1, M_T=0)$ transition, where the initial and final states are isospin analog states. Then $M_{GT}=0$ and only M_F contributes. The Fermi matrix element is easily evaluated and we find

$$\begin{aligned} M_F &= \langle T=1, M_T=0 | T^+ | T=1, M_T=-1 \rangle & (11.29) \\ &= \sqrt{T(T+1) - M_T(M_T+1)} = \sqrt{2} \\ M_F^2 &= 2 & (11.30) \\ ft_{1/2} &= \frac{6221}{2} \cong 3110 \\ \log ft_{1/2} &= 3.5 \,. & (11.31) \end{aligned}$$

Such a strong transition with $\log ft_{1/2} < 3.7$ is termed "superallowed". Generally these are Fermi transitions.

Parity Nonconservation

The classic demonstration that parity is not conserved by the weak interaction involves the process of nuclear beta decay. One begins by preparing a polarized initial nucleus (e.g. initial spins aligned along $+\hat{z}$). The rate of β emission relative to the spin direction ($\hat{z}$) is measured. The rate as a function of the angle relative to the spin direction $\hat{J}$ is given by

$$d\omega \propto \left(1 + \alpha \frac{\hat{J} \cdot \vec{P}_e}{E_e}\right) \,. \tag{11.32}$$

The quantity $\hat{J} \cdot \vec{P}_e$ is a pseudoscalar, and the fact that the rate depends on this pseudoscalar must be due to the fact that parity symmetry is not conserved by the decay process.
Example (1): ^{60}Co at 0.01° inside solenoid at high B field.

The nuclear polarization is $\propto \frac{\mu B}{kT}$. One measures the angular distribution of β^- emission relative to the B-field direction. Experimentally, the value of $\alpha = -1$ is measured. This indicates that the β^- is preferentially emitted opposite to the $\hat{J}$ direction. The explanation is that the parity

non-conserving weak interaction always creates β^- (and neutrinos) with negative helicity (i.e., left-handed). In addition, the theory predicts that anti-neutrinos (and β^+) are emitted with positive helicity (right-handed). This fact is also verified in nuclear beta decay experiments.
Example (2): Neutrino helicity [Goldhaber-Grodzins-Sunyar experiment]

In this experiment, the electron capture process $^{152}\mathrm{Eu}(J=0) \rightarrow ^{152}\mathrm{Sm}^*(J=1)+\nu$ is studied. Thus, by angular momentum conservation the $^{152}\mathrm{Sm}^*$ spin is opposite of ν. The $^{152}\mathrm{Sm}^*(J=1)$ state then gamma decays

$$^{152}\mathrm{Sm}^*(J=1) \rightarrow ^{152}\mathrm{Sm}(J=0)+\gamma \tag{11.33}$$

and the γ must carry the spin of the $^{152}\mathrm{Sm}^*(J=1)$ state. The experiment is to measure the helicity of γ's emitted in the direction of the recoiling $^{152}\mathrm{Sm}^*$ using a magnetized Fe absorber. The experimental result verifies that the ν_e is emitted with negative helicity.

11.2 Neutrino Oscillations

We begin with a brief introduction to the physics of neutrino oscillations in free space. We discuss the case of two flavors of neutrino, ν_μ and ν_e. The generalization to three flavors is straightforward. These neutrinos are those created (and absorbed) via weak interaction processes. However, we postulate that they are not the mass eigenstates. Rather, they are a mixture of two mass eigenstates designated ν_1 and ν_2 with masses m_1 and m_2 ($m_1 \neq m_2$). The weak interaction states are obtained by a unitary transformation of these mass eigenstates:

$$|\nu_e\rangle = \cos\theta|\nu_1\rangle + \sin\theta|\nu_2\rangle \tag{11.34}$$

$$|\nu_\mu\rangle = -\sin\theta|\nu_1\rangle + \cos\theta|\nu_2\rangle \tag{11.35}$$

where θ is a mixing angle and a parameter of the theory. A weak interaction process like nuclear beta decay generates a ν_e, which then propagates as a function of time as

$$|\nu(t)\rangle = e^{-iE_1 t}\cos\theta|\nu_1\rangle + e^{-iE_2 t}\sin\theta|\nu_2\rangle\,. \tag{11.36}$$

At $t=0$ we have a pure ν_e but because of the phase slippage as a function of time, the relative degree of ν_μ and ν_e in the state vector varies. If the mass difference is small, $\Delta m^2 \equiv m_2^2 - m_1^2 \ll p^2$ ($p \cong E_1 \cong E_2$ is the momentum) then the energies are related by

$$E_1 - E_2 \cong \frac{m_2^2 - m_1^2}{2p}\,. \tag{11.37}$$

Then the probabilities for detecting a ν_e or ν_μ at a distance $x(=t)$ are given by

$$P_e(x) = |\langle\nu_e|\nu\rangle_t|^2 = 1 - \sin^2 2\theta \sin^2\left(\frac{\pi x}{L}\right) \tag{11.38}$$

$$P_\mu(x) = |\langle\nu_\mu|\nu\rangle_t|^2 = \sin^2 2\theta \sin^2\left(\frac{\pi x}{L}\right) \tag{11.39}$$

where the characteristic oscillation length (in vacuum) is defined by

$$L \equiv \frac{4\pi p}{\Delta m^2}\,. \tag{11.40}$$

Figure 11.4: Distribution of observed atmospheric neutrino events vs. zenith angle from the SuperKamiokande experiment, compared with Monte Carlo simulations. The blue hatched region represents the prediction without neutrino oscillations and the red line includes the effect neutrino oscillations. (PC means 'partially contained' events.)

This two flavor approximation is a useful approximation for analysis of many experiments. The generalization to three generations involves a 3×3 mixing matrix:

$$|\nu_\ell\rangle = \sum_i U_{\ell i} |\nu_i\rangle \tag{11.41}$$

where ℓ is a flavor index (e, μ, τ) and i corresponds to the mass eigenstate $(i = 1, 2, 3)$. The mixing matrix is usually parametrized by three angles, conventionally denoted as $\theta_{12}, \theta_{13}, \theta_{23}$, one CP violating phase δ and two Majorana phases α_1, α_2. Using c for the cosine and s for the sine, we write U as

$$\begin{pmatrix} \nu_e \\ \nu_\mu \\ \nu_\tau \end{pmatrix} = \begin{pmatrix} c_{12}c_{13} & s_{12}c_{13} & s_{13}e^{-i\delta} \\ -s_{12}c_{23} - c_{12}s_{23}s_{13}e^{i\delta} & c_{12}c_{23} - s_{12}s_{23}s_{13}e^{i\delta} & s_{23}c_{13} \\ s_{12}s_{23} - c_{12}c_{23}s_{13}e^{i\delta} & -c_{12}s_{23} - s_{12}c_{23}s_{13}e^{i\delta} & c_{23}c_{13} \end{pmatrix} \begin{pmatrix} e^{i\alpha_1/2}\,\nu_1 \\ e^{i\alpha_2/2}\,\nu_2 \\ \nu_3 \end{pmatrix} . \tag{11.42}$$

Here, for example $s_{12} = \sin\theta_{12}$ and so on. There are 3 corresponding mass differences Δm^2_{12}, Δm^2_{13} and Δm^2_{23}. This matrix is analagous to the CKM matrix used to describe the charged weak interactions of the quarks.

The first experimental observation of neutrino oscillations was due to the SuperKamiokande experiment, located deep underground in Japan. This large (22 kTon) water Cerenkov detector

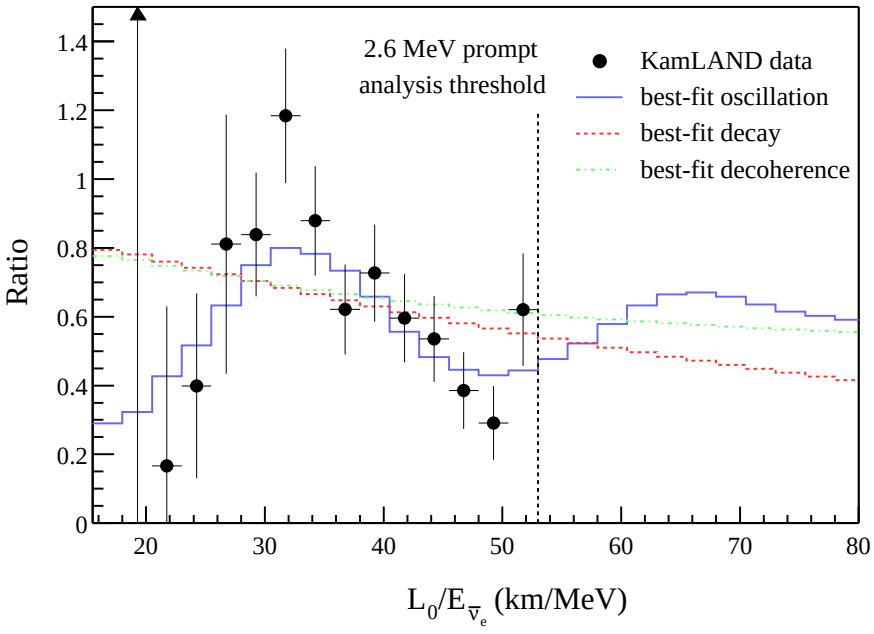

Figure 11.5: Ratio of the observed $\bar{\nu}_e$ spectrum to the no-oscillation expectation, vs. L_0/E from the KamLAND experiment. The curves show best fits to the oscillation hypothesis, neutrino decay, and neutrino decoherence models. $L_0 = 180$ km is the average baseline.

was used to observe neutrinos created in the upper atmosphere by cosmic rays. The Cerenkov detector was capable of distinguishing electron-like events (showering events that produced "fuzzy" Cerenkov ring structures) from muon-like events (non-showering events that produced "sharp" rings). It was observed that there was a deficit of muon type events in the upward direction (neutrinos produced $\sim 10,000$ km away) relative to the downward muon-type events (produced only ~ 100 km away. The electron type events were detected at the expected rates from all directions. The data are shown in Figure 11.4. The interpretation of these observations is that the muon neutrinos are disappearing due to oscillations over a distance scale of several thousand kilometers. Since it appears that the muon neutrinos disappear and there is no evidence for an enhancement of the electron neutrinos, this oscillation presumably involves mostly ν_τ appearance (these are not observed due to the high threshold for τ production). Thus, this oscillation is identified as the 23 oscillation, with the corresponding $\Delta m^2_{23} \simeq 2.5 \times 10^{-3}$ eV^2 (from the analysis of the oscillation length L_{23}. The 23 mixing is close to maximal: $\sin\theta_{23} \simeq 1$.

The 12 oscillation has also been observed, using $\bar{\nu}_e$ from nuclear reactors. The KamLAND experiment used a large liquid scintillator detector (also located in the Kamioka mine in Japan) to study the disappearance of $\bar{\nu}_e$ from the nuclear power reactors in Japan. The average baseline to these reactors was about 180 km, and the energy dependence of the observed oscillation probability (see Figure 11.5) was used to determine that $\Delta m^2_{12} \simeq 7.9 \times 10^{-5}$ eV^2. The corresponding mixing angle is $\sin\theta_{12} \simeq 0.5$

11.3 Matter Enhanced Oscillations

In dense matter (like the solar interior), there is a substantial density of electrons present. The ν_e interact with electrons differently than do the ν_μ. This affects the phase slippage of ν_e relative to ν_μ and can have a dramatic effect on the flavor transformation dynamics.

It is useful to recast the oscillation formulae in a matrix form as follows. (We will simplify this discussion to just 2 flavors.) The transformation between basis states can be written ($C \equiv \cos\theta,\ S \equiv \sin\theta$)

$$\begin{pmatrix} \nu_e \\ \nu_\mu \end{pmatrix} = \begin{pmatrix} C & S \\ -S & C \end{pmatrix} \begin{pmatrix} \nu_1 \\ \nu_2 \end{pmatrix} \tag{11.43}$$

with the inverse transformation

$$\begin{pmatrix} \nu_1 \\ \nu_2 \end{pmatrix} = \begin{pmatrix} C & -S \\ S & C \end{pmatrix} \begin{pmatrix} \nu_e \\ \nu_\mu \end{pmatrix}. \tag{11.44}$$

The time evolution of the mass eigenstates can be written

$$|\nu_i(t)\rangle = e^{-i(E_i - p)t}|\nu_i(0)\rangle \tag{11.45}$$

$$= e^{-im_i^2 t/2p}|\nu_i(0)\rangle; \quad i = 1, 2, \tag{11.46}$$

or

$$\frac{d|\nu_i\rangle}{dt} = -i\frac{m_i^2}{2p}|\nu_i\rangle. \tag{11.47}$$

Therefore, we can express the time evolution in the $\{\nu_e,\ \nu_\mu\}$ basis as

$$i\frac{d}{dt}\begin{pmatrix} \nu_e \\ \nu_\mu \end{pmatrix} = \begin{pmatrix} C & S \\ -S & C \end{pmatrix} i\frac{d}{dt}\begin{pmatrix} \nu_1 \\ \nu_2 \end{pmatrix} \tag{11.48}$$

$$= \frac{1}{2p}\begin{pmatrix} C & S \\ -S & C \end{pmatrix}\begin{pmatrix} m_1^2 & 0 \\ 0 & m_2^2 \end{pmatrix}\begin{pmatrix} \nu_1 \\ \nu_2 \end{pmatrix} \tag{11.49}$$

$$= \frac{1}{2p}\begin{pmatrix} C^2m_1^2 + S^2m_2^2 & CS\Delta m^2 \\ CS\Delta m^2 & C^2m_2^2 + S^2m_1^2 \end{pmatrix}\begin{pmatrix} \nu_e \\ \nu_\mu \end{pmatrix}. \tag{11.50}$$

The effect of dense matter is then included by modifying the diagonal matrix element

$$C^2m_1^2 + S^2m_2^2 \to C^2m_1^2 + S^2m_2^2 + 2\sqrt{2}G_F n_e p \tag{11.51}$$

where n_e is the number of e^- per unit volume. If we now define

$$L_0 \equiv \frac{2\pi}{\sqrt{2}G_F n_e} \tag{11.52}$$

the solutions (for fixed n_e) can be rewritten as

$$|\langle\nu_e|\nu(t)\rangle|^2 = 1 - \sin^2 2\theta_m \sin^2\frac{\pi x}{L_m} \tag{11.53}$$

$$|\langle\nu_\mu|\nu(t)\rangle|^2 = \sin^2 2\theta_m \sin^2\frac{\pi x}{L_m} \tag{11.54}$$

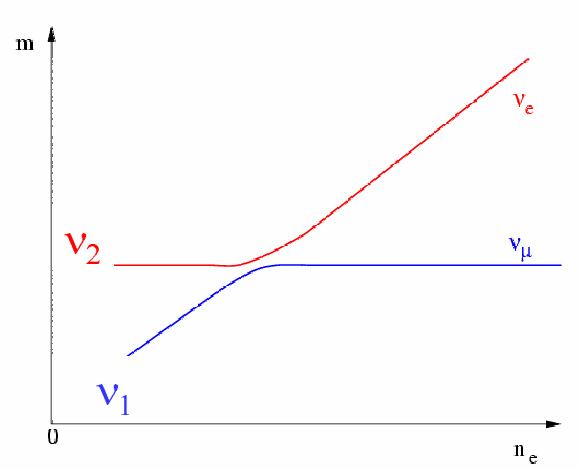

Figure 11.6: Schematic plot of the energy levels of neutrino states as a function of the density of electrons.

with

$$L_m \equiv L\left[1 - 2\frac{L}{L_0}\cos 2\theta + \left(\frac{L}{L_0}\right)^2\right]^{-\frac{1}{2}} \tag{11.55}$$

and

$$\tan 2\theta_m = \frac{\sin 2\theta}{(\cos 2\theta - L/L_0)}\,. \tag{11.56}$$

It is instructive to consider some simple limiting cases. In the case $L \ll L_0$ (e.g., at low density n_e), the length scale for the effect of neutrino matter interactions is much greater than the oscillation length. On the other hand, if $L \gg L_0$ (e.g. at extremely high densities) the interaction length with matter is so short that oscillations do not get the chance to develop. Then $\theta_m \to 0$ and we have $|\nu_e\rangle \cong |\nu_1\rangle$ and $|\nu_\mu\rangle \cong |\nu_2\rangle$. The most interesting region of n_e is where $L \sim L_0$. In fact an important special case is where $L = L_0 \cos 2\theta$, where θ_m becomes 45°.

As the n_e propagate through the solar interior, they go from a region of high n_e where $L > L_0$ through the resonant region $L \sim L_0$ to a region of low density. Thus they begin as essentially $|\nu_1\rangle$, the heavier mass state ($m_1 > m_2$). As they go to the lower density region $L < L_0$, they pass through the resonance region, where the level crossing is indicated in the diagram. The levels to not actually cross due to the effective repulsion of the off-diagonal terms in the Hamiltonian. If the transition is gradual enough, then the ν_e adiabatically becomes a ν_μ depleting the ν_e flux. Since

the expression for L/L_0 is momentum dependent

$$\frac{L}{L_0} = \frac{2\sqrt{2}G_F n_e p}{\Delta m^2} \tag{11.57}$$

the conversion $\nu_e \to \nu_\mu$ is energy dependent. In fact, if the value of Δm^2 is about right then the low energy neutrinos have $L/L_0 \ll 1$ in the solar interior and only the higher energy neutrinos undergo a transformation.

This explanation was dramatically verified by the Sudbury Neutrino Observatory (SNO) experiment. The SNO experiment combines the now high-developed capability of water Čerenkov detectors with the unique opportunities afforded by using deuterium to detect the solar neutrinos [**?**, **?**]. Low energy neutrinos can dissociate deuterium via the charged current (CC) reaction

$$\nu_e + d \to e^- + 2p \tag{11.58}$$

or the neutral current (NC) reaction

$$\nu_\ell + d \to \nu_\ell + p + n\,. \tag{11.59}$$

Only ν_e can produce the CC reaction, but all flavors $\ell = e, \mu, \tau$ can contribute to the NC rate. The CC reaction is detected via the energetic spectrum of e^- which closely follows the ^{8}B solar ν_e spectrum. The NC reaction involves three methods for detection of the produced neutron: (a) capture on deuterium and detection of the 6.25 MeV γ-ray, (b) capture on Cl (due to salt added to the D_2O) and detection of the 8.6 MeV γ-ray, or (c) capture in ^{3}He proportional counters immersed in the detector. There are also some events associated with the elastic scattering of the solar-ν on e^- in the detector which is dominated by the charged current reaction (again only ν_e) but has some $\sim 20\%$ contribution from neutral currents (all flavors equally contribute).

The SNO collaboration has published data on the CC and NC rate (from processes (a) and (b)). Additional data from the NC process (c) will be forthcoming in the future. Nevertheless, the reported results (see Fig. 11.7) demonstrate very clearly that the total neutrino flux ($\nu_e + \nu_\mu + \nu_\tau$ as determined from NC) is in good agreement with the SSM, but that the ν_e flux is suppressed (as determined from CC). This represents rather definitive evidence that the ν_e suppression is due to flavor-changing processes that convert the ν_e to the other flavors, as expected from ν-oscillations. The SNO results can be combined with the other solar neutrino data to provide constraints on the parameters θ_{12} and Δm^2_{12}. The solar neutrino results can then be compared with the results of the KamLAND experiment, as shown in Fig. 11.8. The remarkable agreement is what one would expect if CPT were conserved, so that the neutrinos and antineutrinos exhibited the same masses and mixing parameters. The combined analysis of solar neutrino data and KamLAND (assuming CPT invariance) provides an impressive determination of the 12 oscillation parameters:

$$\Delta m^2_{12} = 7.9^{+0.6}_{-0.5} \times 10^{-5}\ \text{eV}^2\,, \tag{11.60}$$

$$\tan^2\theta_{12} = 0.40^{+0.10}_{-0.07}\,. \tag{11.61}$$

11.4 Double Beta Decay

Double beta decay is a rare transition between two nuclei with the same mass number A involving change of the nuclear charge Z by two units. The decay can proceed only if the initial nucleus

Figure 11.7: Measured solar neutrino fluxes from SNO for the NC and CC processes, along with elastic scattering events (ES) and the standard solar model prediction .

is less bound than the final one, and both must be more bound than the intermediate nucleus. These conditions are fulfilled in nature for many even-even nuclei, due to the nature of the pairing interaction as discussed in Chapter 9. Fig. 11.9 shows a typical situation for $A = 136$. Typically, the decay can proceed from the ground state (spin and parity always 0^+) of the initial nucleus to the ground state (also 0^+) of the final nucleus, although the decay into excited states (0^+ or 2^+) is in some cases also energetically possible.

There are, in principle, two types of double beta decay: $2\nu\beta\beta$ where 2 neutrinos and 2 β particles are emitted in the final state, and $0\nu\beta\beta$ where only the 2 β particles are emitted. The two-neutrino decay, $2\nu\beta\beta$,

$$(Z, A) \rightarrow (Z + 2, A) + e_1^- + e_2^- + \bar{\nu}_{e1} + \bar{\nu}_{e2} \tag{11.62}$$

conserves not only electric charge but also lepton number. On the other hand, the neutrinoless decay,

$$(Z, A) \rightarrow (Z + 2, A) + e_1^- + e_2^- \tag{11.63}$$

violates lepton number conservation. One can distinguish the two decay modes by the shape of the electron sum energy spectra, which are determined by the phase space of the outgoing light particles. Since the nuclear masses are so much larger than the decay Q value, the nuclear recoil energy is negligible, and the electron sum energy of the $0\nu\beta\beta$ is simply a peak at $T_{e1} + T_{e2} = Q$ smeared only by the detector resolution.

The $2\nu\beta\beta$ decay is an allowed process with a very long lifetime $\sim 10^{20}$ years, and has now been experimentally observed in several nuclei cases. This is a standard second order weak interaction process, and is a significant challenge for nuclear theory to calculate the lifetimes.

The $0\nu\beta\beta$ decay involves a vertex changing two neutrons into two protons with the emission of two electrons and nothing else. The total energy of the two electrons is a constant determined by the

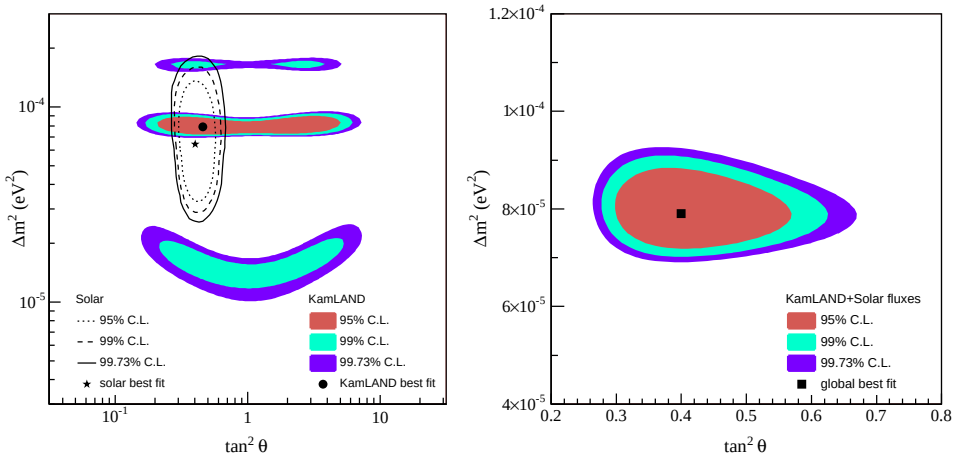

Figure 11.8: Allowed regions in Δm^2 and $\tan^2\theta$ for the solar neutrino measurements and KamLAND (antineutrinos). The agreement of the two determinations supports CPT invariance, and by assuming CPT invariance one can produce a combined determination of the oscillation parameters.

initial and final nuclear masses. There are no confirmed experimental observations of $0\nu\beta\beta$ decay to date, but this is an active area of experimental research. As shown in Figure 11.10 the $0\nu\beta\beta$ decay can proceed only when neutrinos are Majorana particles, i.e., they are their own antiparticle. In addition, the left-handed nature of the charged weak interaction at both vertices implies that the right-handed antineutrino must be reabsorbed as a left-handed neutrino. This generally requires that the Majorana neutrino have non-zero mass. Thus the experimental observation of 0ν double beta decay would have profound implications for our knowledge of the properties of neutrinos.

The decay rate for 0ν double beta decay can be written

$$[T^{0\nu}_{1/2}(0^+ \to 0^+)]^{-1} \;=\; G^{0\nu}(E_0, Z) \left| M^{0\nu}_{GT} - \frac{g_V^2}{g_A^2} M^{0\nu}_F \right|^2 \langle m_{\beta\beta} \rangle^2 \;, \tag{11.64}$$

where $G^{0\nu}$ is the exactly calculable phase space integral, $\langle m_{\beta\beta}\rangle$ is the effective neutrino mass and $M^{0\nu}_{GT}$, $M^{0\nu}_F$ are the nuclear matrix elements.

The effective neutrino mass is

$$\langle m_{\beta\beta} \rangle = | \sum_i |U_{ei}|^2 m_{\nu_i} e^{i\alpha_i} | \;, \tag{11.65}$$

where the sum is only over light neutrinos ($m_i < 10$ MeV) The Majorana phases α_i were defined earlier in Eq.(11.42). If the neutrinos ν_i are CP eigenstates, α_i is either 0 or π. Due to the presence of these unknown phases, cancellation of terms in the sum in Eq.(11.65) is possible, and $\langle m_{\beta\beta}\rangle$ could be smaller than any of the m_{ν_i}.

Obviously, any uncertainty in the nuclear matrix elements would be reflected as a corresponding uncertainty in the $\langle m_{\beta\beta}\rangle$. Thus the continued study of these matrix elements is an important topic for nuclear theory.

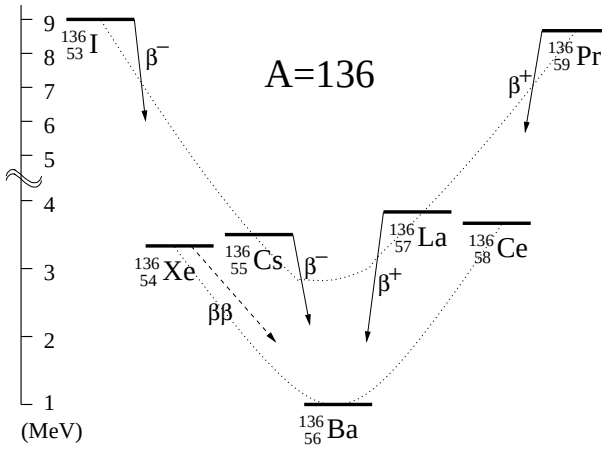

Figure 11.9: Masses of nuclei with $A = 136$. The even-even and odd-odd nuclei are connected by dotted lines. ^{136}Xe is stable against ordinary β decay, but unstable against $\beta^-\beta^-$ decay. The same is true for ^{136}Ce, however, the $\beta^+\beta^+$ decay is expected to be slower than the $\beta^-\beta^-$ decay.

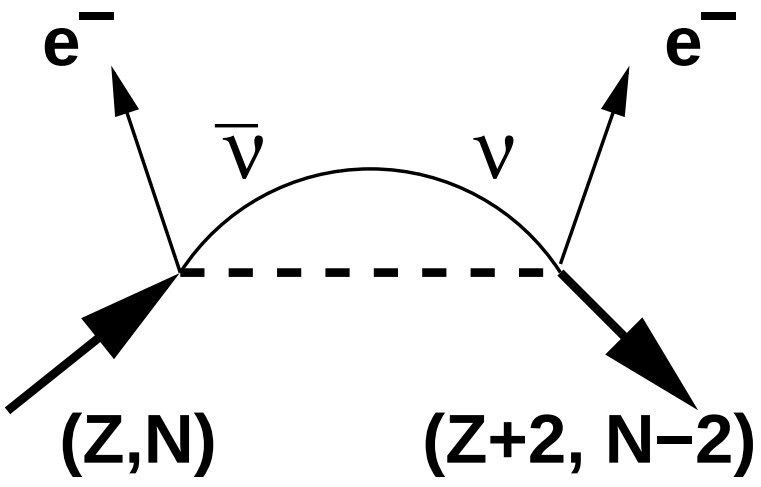

Figure 11.10: Feynman diagram of the double beta decay process. Note that 2 neutrons are converted to 2 protons and 2 electrons are emitted, which violates total lepton number. The intermediate nuclear state is indicated by the dashed line. The emitted antineutrino must be reabsorbed as a neutrino, so this process requires that the neutrino be its own antiparticle.

Chapter 12

Supernova, Neutron Star and Black Hole

For a star with mass larger than 10 solar masses, it undergoes all stages of nuclear burning and eventually develops an iron core. As the mass of the iron core reaches Chandrasekhar limit, it becomes unstable and will collapse under two mechanisms. First, because of the enormous heat, the energy of the photon is high-enough to produce photo-disintegration of iron. Second, the energy of the electron becomes so large that it is viable to have inverse beta reaction, generating neutrons and neutrinos. Therefore, the star will rapidly collapses into a neutron star or a black hole. The gravitational energy released through the processes will produce a huge explosion which is the supernova type II or Ib. In this Chapter, we discuss the supernova explosion phenomena and discuss the heavy nucleus generation, the physics of neutron star and black hole.

12.1 Collapse of a Well-Burned Star into a Neutron Star

When a star is massive enough, after the nuclear burning resulting the iron core, the star cannot have any further nuclear fusion. However, under the gravitational pressure, the star will shrink future, and at some point, it becomes more profitable to turn the protons into neutrons.

Now note that (for a fixed radius r) the electron and gravitational energy of the star increases with increasing x for both non-relativistic (NR) and relativistic (Rel) electron gases:

$$\text{NR}: \qquad E \sim x^{5/3} \tag{12.1}$$

$$\text{Rel}: \qquad E \sim x^{4/3}. \tag{12.2}$$

So it is energetically favorable if we can decrease x through the weak process

$$e^- + p \to n + \nu_e \, . \tag{12.3}$$

At large enough density, the Fermi energy of the electrons exceeds the mass difference $M_n - M_p$ and this process spontaneously proceeds to convert the star to "neutron matter." For a non-relativistic electron gas, we set the Fermi energy to about 1 MeV and using the expression

$$E_F = \frac{\hbar^2}{2m_e}\left(3\pi^2 x \frac{n}{\Omega}\right)^{2/3} \tag{12.4}$$

we obtain the density

$$\frac{n}{\Omega} = 9 \times 10^{30}/\mathrm{cm}^3 \tag{12.5}$$

$$\rho \cong 1.5 \times 10^7 \ \mathrm{g/cm}^3. \tag{12.6}$$

For relativistic electrons $E_F = 2$ MeV implies the density $\rho \cong 10^8$ g/cm^3. Thus, for $\rho > 10^8$ g/cm^3 we expect the protons to convert to neutrons and the star will consist of neutron matter.

We can then write the total energy as the sum of neutron kinetic energy, electron kinetic energy, and the gravitational potential energy:

$$E(r,\ x) = \frac{3\hbar^2(1-x)n}{10M_p r^2}\left(\frac{9\pi(1-x)n}{4}\right)^{2/3} + \frac{3\hbar x n}{4r}\left(\frac{9\pi x n}{4}\right)^{1/3} - \frac{3}{5}G\frac{n^2M_p^2}{r}. \tag{12.7}$$

We then require the following conditions for an equilibrium configuration:

$$\frac{\partial E}{\partial r} = 0 \tag{12.8}$$

$$\frac{\partial E}{\partial x} = 0. \tag{12.9}$$

Assuming that the matter predominantly converts to neutrons we choose $x = 0$ and obtain the equilibrium radius

$$r_{\mathrm{eq}} = \frac{\hbar^2}{GnM_p^3}\left(\frac{9\pi n}{4}\right)^{2/3}. \tag{12.10}$$

For $n = 1.2 \times 10^{57}$ $(1\ M_\odot)$ we obtain the values

$$r_{eq} = 1.24 \times 10^6 \ \mathrm{cm} = 1.24 \times 10^4 \ \mathrm{m} = 1.24 \ \mathrm{km} \tag{12.11}$$

$$\Omega = 7.96 \times 10^{18} \ \mathrm{cm}^3 \tag{12.12}$$

$$\rho = 2.5 \times 10^{14} \ \mathrm{g/cm}^3 \tag{12.13}$$

Plugging this r_{eq} into $E(r_{eq},\ x)$ and requiring

$$\frac{\partial E(r_{eq},\ x)}{\partial x} = 0 \tag{12.14}$$

yields the value $x = 0.005$. Thus we find a consistent solution with $x \sim 0$ and $\rho \sim \rho_{NM}$ with a radius of $r_{eq} \sim 1$ km. *This is a large nucleus at nuclear matter density, consisting of neutrons only, with a radius of 1 km!*

We now include nuclear interactions and use the parametrization of the Bethe-Weizsäcker formula:

$$\frac{E}{n} \cong a_A(\rho) - a_V(\rho) - \frac{3}{5}G\left[\frac{4\pi M^2 M_p^4}{3}\rho\right]^{1/3} \tag{12.15}$$

where we have assumed $x = 0$ and $\rho = \frac{n}{\Omega}$=# nucleons/cm^3. We need to consider the two regions of density:

- (a) For $\rho = \rho_0 = 1.4 \times 10^{38}/\text{cm}^3$, we know that $a_A - a_V \cong 7.5$ MeV=7.5×10^{-3} GeV from the empirical fits to normal nuclei. This implies a minimum star mass for $\frac{E}{n} < 0$

$$M > \frac{1}{M_p^2}\left(\frac{3}{4\pi\rho_0}\right)^{1/3}\left(\frac{5(a_A - a_V)}{3G}\right)^{3/2} = 0.04\ \text{M}_\odot \tag{12.16}$$

  or $n = 4.3 \times 10^{55}$ with $r = \left(\frac{3n}{4\pi\rho}\right)^{1/3} = 4$ km.

- (b) For $\rho > \rho_0$, we need the ρ dependence of $\frac{B}{A} = a_V - a_A$.

Empirically (from measurements of the "breathing mode" of nuclei) and from calculations based on nuclear matter theory (more later) we find the "compressibility":

$$K = -k_f^2\frac{d^2(B/A)}{dk_f^2} = -9\rho_0^2\frac{d^2(B/A)}{d\rho^2} = 0.1 - 0.2\ \text{GeV}. \tag{12.17}$$

Using this parameter we can approximately describe the compression of nuclear matter by the expression

$$\frac{B}{A} = \left(\frac{B}{A}\right)_0 - \frac{K}{18\rho_0^2}(\rho - \rho_0)^2\,. \tag{12.18}$$

Then we obtain the equilibrium condition for neutron star stability as

$$\frac{d}{d\rho}\left(\frac{E}{n}\right) = \frac{K}{9\rho_0^2}\rho - \frac{1}{5}G\left[\frac{4\pi M^2 M_p^4}{3\rho^2}\right]^{1/3} = 0 \tag{12.19}$$

which yields the density

$$\rho = \left(\frac{9\rho_0^2 G}{5K}\right)^{3/5}\left(\frac{4\pi M^2 M_p^4}{3}\right)^{1/5}\,. \tag{12.20}$$

If we now take $M = 1.5\ \text{M}_\odot$ we find

$$\rho \cong (1.6 - 2.4) \times 10^{38}\text{cm}^{-3} = (1.1 - 1.7)\rho_0\,. \tag{12.21}$$

In fact more realistic calculations give $\rho \sim 4 - 5\ \rho_0$ and $x \sim$0.15. Nevertheless, our simple approximations do illustrate the basic physical principles of the structure of neutron stars.

12.2 Supernova Explosion and R-process

In Type II supernova, mass flows into the core by the continued making of iron, the most stable nucleus, from nuclear fusion. Once the core has gained so much mass that it cannot withstand its own weight (Chandrasekar limit), the core implodes. This implosion can usually be brought to a halt by neutrons, the only things in nature that can stop such a gravitational collapse. When the collapse is abruptly stopped by the neutrons, matter bounces off the hard iron core, thus turning the implosion into an explosion, ejecting the star mantle.

Therefore, the supernova explosion is characterized by electron captures and neutrino release. In fact, almost all of the energy of the supernova II and Ib and Ic explosions is released in the

form of the neutrinos. The fundamental problem in understanding the supernova explosion is the energy transfer process in which the free fall energy transfers into the star mantle and resulting in an explosion. The detailed study shows that it is a very difficult problem. Numerical simulations have difficulty to create an explosion.

One of the most important function of the supernova explosion is to create heavy elements in the Universe. These elements cannot be produced in the usual star fusion processes and must be produced in the unusual environment such as R-process.

The R-process (R for rapid) is a neutron capture process for radioactive elements which occurs in high neutron density, high temperature conditions. In the R-process nuclei are bombarded with a large neutron flux to form highly unstable neutron rich nuclei which very rapidly decay to form stable neutron rich nuclei.

A primary site of the R-process is believed to be iron-core collapse supernovae, which provide the necessary physical conditions for the R-process. However, the abundance of R-process elements requires that either only a small fraction of supernova return R-process elements to the outside or that each supernova only contributes a very small amount of R-process elements.

Due to the much higher neutron flux in this process (on the order of 10^{22} neutrons per cm^2 per second), the rate of isotopic formation is much faster than the beta decays which follow, meaning that this process "runs up" along the neutron drip line (a line alone with adding more neutrons will not lead to a stable nucleus) with the only two hold-ups being closed neutron shells extending the time it takes to create new isotopes, and the degree of nuclear stability in the heavy-isotope region, which terminates the R-process when such nuclei become readily unstable to spontaneous fission (currently believed to be in the region of A = 270 - or roughly in the Rutherfordium - Darmstadtium area of the periodic table).

Elemental abundance peaks show some support for the idea of rapid neutron capture and delayed beta emission, as the R-process peaks are at about 10 Atomic mass units below those of the S-process peaks (which occur exactly at closed neutron shells), indicating that the "run up" along the neutron drip line reaches closed neutron shells but with sufficient proton deficiency to make the peaks resolvable.

12.3 Neutron Stars

As the result of the type II and type Ib and Ic supernova explosion, a neutron star forms. The concept of a neutron star was suggested by Baade and Zwicky as early as 1933.

A stable neutron star has mass of order 1.35 to 2.1 solar masses, with a radius about 20 to 10 km. The density of the neutron stars is exceedingly large, on the order of 10^14 to 2×10^{15} g/cm^3.

In the core collapsing processes, the angular momentum is almost conserved and therefore, the neutron star has a large angular momentum. Therefore it rotates several times or even hundreds of times a second. However, the rotational axis needs not coincide with the axis of magnetic field. As such, when it rotates, it produces electromagnetic radiation. This radiation is powered by rotation and hence the star is also called "rotation powered pulsar". As the star rotation, one sees a periodic emission of the radiation in one directions. As the radiation carries away the rotational energy, the rotation slows down. However, this process takes a very very long time.

Some of the most interesting questions about the neutron stars have not been settled, which include what is the maximum mass of a neutron star? What is the radius of a neutron star of a given mass, and what is the physical origin of transient phenomena in neutron star?

The maximum mass of a neutron star is a result of gravitational attraction and nuclear repulsion. Since the largest mass star corresponds to a largest nuclear density, this also yields what is the largest nuclear density possible in a star without gravitational collapse. This upper limit clearly indicates a particular class of equation of states for neutron-rich nuclear matter.

Besides the maximum mass, the radius of the neutron star also depends on the equation of state.

For a piece of matter without the problem of gravitational collapse, the ground state of cold matter at extremely high-density might be a color superconductor in a color-flavor-locked phase.

Density dependence of the symmetry energy is an important piece of information characterizing the equation of state for neutron-rich matter. This density dependence might be measurable through measuring the neutron radius of Pb nucleus. Through parity elastic electron scattering on the Pb nucleus, one might be able to learn the density dependence of the symmetry energy.

12.4 Black Holes

When the mass of a neutron star exceeds a certain limit, the degenerate pressure of the neutrons no longer can resist the gravitational pull and the star will continue to collapse to form a black hole. The size of the black hole is determined by its Schwartzschild radius,

$$R = 2GM/c^2 \tag{12.22}$$

which is proportional to its mass. One way to derive this to calculate the escape velocity of an object at distance r,

$$\frac{1}{2}mv^2 = GmM/r \tag{12.23}$$

At the Schwartzschild radius R, the escape velocity equals to the speed of light c. Because of that, even light cannot escape the gravitational pull of a black hole.

As an example, a blackhole with one solar mass has a Schwartzschild radius 3km! A blackhole of 50kg mass has a radius 10^{-10} fm!

Other interesting phenomena associated with black holes include 1) speeding up of the clock as it co-moves with the surface of the collapsing star and 2) the redshift of a photon to zero frequency.

A possible way to observe a black hole is binary systems in which one of them is a neutron star and the other is a black hole. As the mass of the neutron star being sucked into a black hole, there is an X-ray emission. One of the candidate is Cygnus X-1. Another place to look for black holes is at the centers of the galaxies. The center of the Milky Way might contain a black hole of mass 4×10^6 solar masses.

Black hole has temperature. The so-called Hawking temperature of a black hole is

$$kT_H = \frac{\hbar c^3}{8\pi GM} \tag{12.24}$$

which is inversely proportional to its mass. Larger the mass, lower the temperature. Because of this, the black hole has also entropy, which is proportional to its surface area.

An object with finite temperature will radiate according to the black-body radiation formula—it is called Hawking radiation in this context. When it radiates, the mass of the black hole decreases,

and its temperature increases, and eventually all masses radiate away. Therefore, a black hole when left along has a finite life time. It is not difficult to show that the life time of a black hole is

$$\sim G^2 M^3/\hbar c^4 \tag{12.25}$$

which is a very long time for a blackhole of one solar mass.